

Review

Influence of Preparation Characteristics on Stability, Properties, and Performance of Mono- and Hybrid Nanofluids: Current and Future Perspective

Humaira Yasmin ^{1,*}, Solomon O. Giwa ², Saima Noor ¹ and Hikmet Ş. Aybar ^{3,4}

¹ Department of Basic Sciences, Preparatory Year Deanship, King Faisal University, Al-Ahsa 31982, Saudi Arabia

² Department of Mechanical Engineering, Olabisi Onabanjo University, Ago-Iwoye P.M.B. 2002, Nigeria

³ Department of Mechanical Engineering, Eastern Mediterranean University, TRNC, Via Mersin 10, 99628 Famagusta, Turkey

⁴ Department of Medical Research, China Medical University Hospital, China Medical University, Taichung 404, Taiwan

* Correspondence: hhassain@kfu.edu.sa

Abstract: Nanofluids (NFs) synthesized via the suspension of diverse nanoparticles into conventional thermal fluids are known to exhibit better thermal, optical, tribological, and convective properties, photothermal conversion, and heat transfer performance in comparison with traditional thermal fluids. Stability is pivotal to NF preparation, properties, performance, and application. NF preparation is not as easy as it appears, but complex in that obtaining a stable NF comes with the harnessing of different preparation parameters. These parameters include stirring duration and speed, volume, density, base fluid type, weight/volume concentration, density, nano-size, type of mono or hybrid nanoparticles used, type and quantity of surfactant used, and sonication time, temperature, mode, frequency, and amplitude. The effect of these preparation parameters on the stability of mono and hybrid NFs consequently affects the thermal, optical, rheological, and convective properties, and photothermal conversion and heat transfer performances of NFs in various applications. A comprehensive overview of the influence of these preparation characteristics on the thermal, optical, rheological, and properties, photothermal conversion, and heat transfer performance is presented in this paper. This is imperative due to the extensive study on mono and hybrid NFs and their acceptance as advanced thermal fluids along with the critical importance of stability to their properties and performance. The various preparation, characterization, and stability methods deployed in NF studies have been compiled and discussed herein. In addition, the effect of the various preparation characteristics on the properties (thermal, optical, rheological, and convective), photothermal conversion, and heat transfer performances of mono and hybrid NFs have been reviewed. The need to achieve optimum stability of NFs by optimizing the preparation characteristics is observed to be critical to the obtained results for the properties, photothermal conversion, and heat transfer performance studies. As noticed that the preparation characteristics data are not detailed in most of the published works and thus making it mostly impossible to reproduce NF experimental studies, stability, and results; future research is expected to address this gap. In addition, the research community should be concerned about the aging and reusability of NFs (mono and hybrid) in the nearest future.

Keywords: heat transfer performance; NFs; stability; sonication; surfactant fraction; thermal properties



Citation: Yasmin, H.; Giwa, S.O.; Noor, S.; Aybar, H.Ş. Influence of Preparation Characteristics on Stability, Properties, and Performance of Mono- and Hybrid Nanofluids: Current and Future Perspective. *Machines* **2023**, *11*, 112. <https://doi.org/10.3390/machines11010112>

Academic Editors: Javad Mohammadpour and Shahid Husain

Received: 21 December 2022

Revised: 7 January 2023

Accepted: 9 January 2023

Published: 13 January 2023



Copyright: © 2023 by the authors. Licensee MDPI, Basel, Switzerland. This article is an open access article distributed under the terms and conditions of the Creative Commons Attribution (CC BY) license (<https://creativecommons.org/licenses/by/4.0/>).

1. Introduction

The advent of nanotechnology has brought about significant technological advancement in many fields of study. The birth of NFs as advanced thermal fluids in the area of thermal management is a laudable and notable feat. NFs (mono and hybrid) have been extensively researched and proven to be better than conventional thermal fluids, and this is

due to their enhanced thermophysical and convective properties [1–13]. The application of diverse mono and hybrid NFs in various thermal systems has been studied experimentally [5,6,12] and numerically [14–17], and found to improve heat transfer characteristics better than traditional thermal fluids. NFs have been investigated in the various types of convective heat transfer studies, such as natural [18–22], mixed [23,24], and forced convection [25–30] at laminar, turbulent, and transition regimes. These studies showed the enhancement of heat transfer performance with the HNFs found to be better thermal fluids than MNFs. In addition, the use of mono and hybrid NFs in heat transfer systems such as solar collectors [12,31–33], radiators [34–36], refrigerators [37], mini-channel [38], microtubes [39,40], heat pipes [20,41], air-conditioning [42], heat exchangers [43], etc, have been studied. The deployment of NFs in these thermal transporting devices showed improvements in the heat transfer and flow characteristics than when conventional thermal fluids were used. Furthermore, mono and hybrid NFs/NPs have been employed as coolants (metal rolling process and metal machining operation) [44–47], lubricants (automobile) [48–51], thermal storage materials [52–54], sensors [55–57], drilling muds [58,59], chemically enhanced oil recovery material [60–62], etc, and are better thermal fluids/materials than the conventional thermal fluids/materials.

The suspension of diverse NPs into various base fluids to synthesize NFs has been proven to possess superior thermal properties compared with the traditional thermal fluids. Current research progress has revealed that the suspension of HNFs (mixing of two or more NPs) in different base fluids possessed better convective and thermal properties than MNFs [2,4,12]. MNF and HNF preparation appears to be a simple practice but complex in the true sense of it. Stability, which is the even distribution of mono and hybrid NPs in the base fluid, is key to the results associated with the thermal [63,64] and convective properties [65–68] and performance [68–71] of mono and hybrid NFs in various areas of their application. The stability of mono and hybrid NFs has been proven to significantly affect their thermal properties [72–81] and convective heat transfer performances [65,82,83]. The instability is marked by sedimentation and agglomeration of the mono and hybrid NPs suspended in the base fluid. This consequently leads to inaccurate results when the resultant mono and hybrid NFs are deployed in different applications [65,67,69–71,84,85]. This goes to show that obtaining good and desirable stability of mono and hybrid NFs is crucial. However, the stability of mono and hybrid NFs are strongly connected to preparation variables, such as stirring time, rate, temperature, sonication time, power, frequency, amplitude, and dispersion fraction (where a surfactant is used) [7,75,77,81,86–89]. The sonication variables (time, power, mode, frequency, and amplitude) are related to the sonication energy required to achieve homogenized and stable mono and hybrid NFs [74,78,90,91].

Based on the above comments and the available literature in the public domain regarding the influence of stability on the thermal, optical, and rheological properties, photothermal conversion, and performance characteristics of NFs, we thought it necessary to conduct an overview of this laudable subject. The effects of the preparation methods (one- and two-step strategy), sonication characteristics (sonication mode, time, frequency, power/energy density, and amplitude), stirring, and the deployment of surfactants on stability that consequently impact the properties and performance of mono and hybrid NFs in different areas of application have been well compiled and critically reviewed. This is prompted by the need to bring to the front burner the challenges and ways forward concerning the stability of NFs (mono and hybrid) and the attendant problems. A major feature of this review paper is the foremost consideration of mono and hybrid NFs for their stability, heat transfer performances, and thermal properties as influenced by the preparation characteristics. This work is expected to be a good guide for researchers in NF studies toward achieving good stability and improved results. This paper is divided into six parts. The first part is the general introduction of the paper. In the second part, the preparation methods, characterization techniques, and stability monitoring tests for mono and hybrid NFs are highlighted and discussed. Part 3 involves the effects of preparation characteristics of MNFs on their stability, properties (thermal, optical, and rheological),

and performances (photothermal conversion, heat transfer, and solar collector efficiency), while part 4 addresses the influence of the preparation characteristics of HNFs on their stability, thermal, optical, and rheological properties, and heat transfer performances. The challenges and future research directions are discussed in part 5 of this paper. Finally, the conclusion and recommendations are provided in part 6. A schematic diagram of the work carried out in this paper is provided in Figure 1.

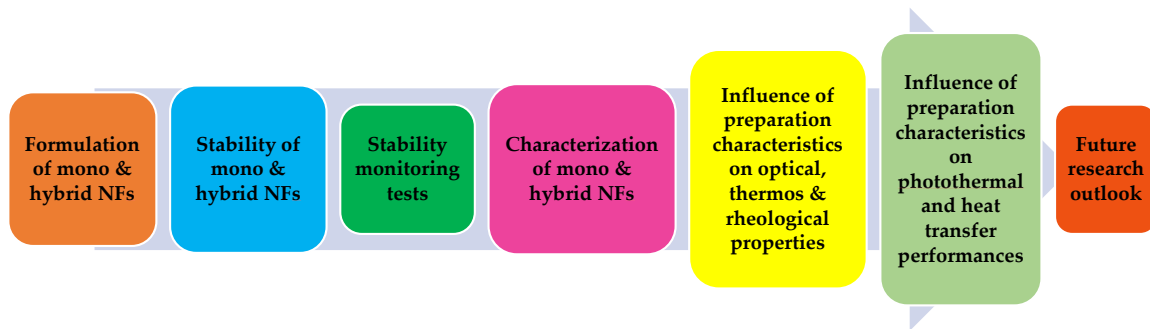


Figure 1. Overview of present study.

2. NF Formulation, Characterization, and Stability

2.1. Formulation Techniques

MNFs and HNFs are formulated through the suspension of MNPs and HNPs, respectively, into conventional thermal fluids, namely, base fluids, of which their stability is very important to the measurement of the thermophysical properties and convective studies. Fundamentally, MNFs and HNFs are formulated using a one- and two-step process (Figure 2). By this, the latter entails two processes, namely, (i) synthesis of MNPs or HNPs in the powdery form and (ii) suspension of MNPs or HNPs into the base fluids. The most reported process in the literature is the two-step process for the formulation of MNFs and HNFs, which can encourage their large-scale formulation at a low cost and an industrial utilization. The shortcoming of the two-step process relates to the sedimentation and agglomeration of MNPs and HNPs due to the Van der Waals forces of attraction among the particles [92]. The one-step process consists of the simultaneous production of MNFs and HNFs by way of synthesis and suspension of MNPs and HNPs in the base fluids. This technique is advantageous as it improves the homogeneity and stability of MNFs and HNFs and eliminates arduous procedures, such as drying and storing in comparison with the single-step process by reducing the agglomeration tendency of MNPs and HNPs [92,93]. However, the industrial application of this technique is impracticable except for low vapor-pressure fluids. This technique is also not cost-effective [94]. In addition, various one-step process techniques have been reported in the literature [93,95,96].

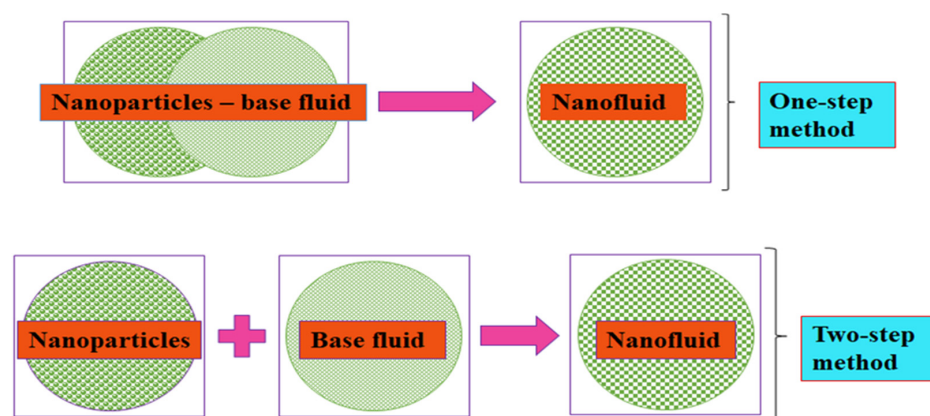


Figure 2. Mono and hybrid NF formulation strategies.

2.2. Characterization Techniques

Numerous techniques have been reported in the literature for the characterization of MNFs and HNFs for their MNP and HNP shapes, sizes, distribution, functional groups, crystalline structure, surface morphology, dispersion, elemental composition, saturation, magnetization, etc. These techniques include Raman spectroscopy, X-ray diffractometer, high-resolution transmission electron microscopy, Fourier transform infrared spectroscopy, scanning electron microscopy, vibrating sample magnetometer, energy-dispersive X-ray spectroscopy, light scattering, and transmission electron microscopy [1,17,78,97–101]. The most used technique for characterizing MNFs and HNFs is transmission electron microscopy (TEM), followed by scanning electron microscopy (SEM) and the X-ray diffractometer (XRD). These most used techniques are often engaged as a stand-alone technique or with other techniques for MNF and HNF characterization. TEM is used to determine the size, shape, and dispersion of MNPs and HNPs in MNFs and HNFs, respectively, while the SEM detects surface morphology and elemental mapping. XRD is used to show the crystalline structure and grain size of MNPs and HNPs contained in MNFs and HNFs, respectively.

2.3. Stability Improvement and Tests

2.3.1. Stability of NFs

The suspension of MNPs and HNPs in various base fluids introduces charges into the base fluids, which leads to the formation of an electrical double layer (EDL) around the particle surface [102]. Therefore, MNFs and HNFs are referred to as electrically conducting fluids. By applying a potential across these fluids, oppositely charged electrodes tend to attract the MNPs or HNPs and EDL. The formation of EDL is strongly connected to the volume fraction, size, surface charge of the particles, and concentration of ions in the base fluids. The stability and even distribution of MNPs or HNPs in the base fluids are vital in the application of MNFs and HNFs because the thermophysical (mostly κ and μ) and optical properties, and the efficiency of the same are significantly related to the concentration of MNPs or HNPs in the suspension [103,104]. Improving the stability of MNFs and HNFs to reduce agglomeration and sedimentation with the two-step process has led to the utilization of four techniques, namely, ultrasonication, surfactant addition, surface modification, and pH control.

2.3.2. Stability Improvement Techniques

Sonication

Sonication is one of the techniques deployed to obtain homogeneous mixtures of NPs suspended in selected base fluids. Several studies demonstrated that sonication affected κ , absorbance wavelength, μ , cluster size, surfactants, the diameter of CNTs, and particle size [74,78,79,85,105–107]. For NFs, a sonication time spanning a few minutes to several hours has been documented. It can be deduced that an optimum sonication time (mainly due to the Brownian motion of MNPs or HNPs) occurred where the variable investigated either reduced (for μ and κ) or increased (for CNT diameter, particle, and cluster size). An optimum sonication time ranging from 12 min [108] to 60 h [105] has been reported in the literature for MNFs and HNFs. This reflects the need to optimize sonication time as it relates to other variables to achieve improved stability. However, this is mostly not the case for most of the studies on the formulation of MNFs and HNFs, except for very limited studies that have optimized the sonication parameters [74,85,109]. Sonication of NFs has been reported to be carried out using the following three different types of ultrasonicators: probe-type, sonication-bath type, and shaker-type [68,80,110]. Figure 3 shows the sonication of HNF.

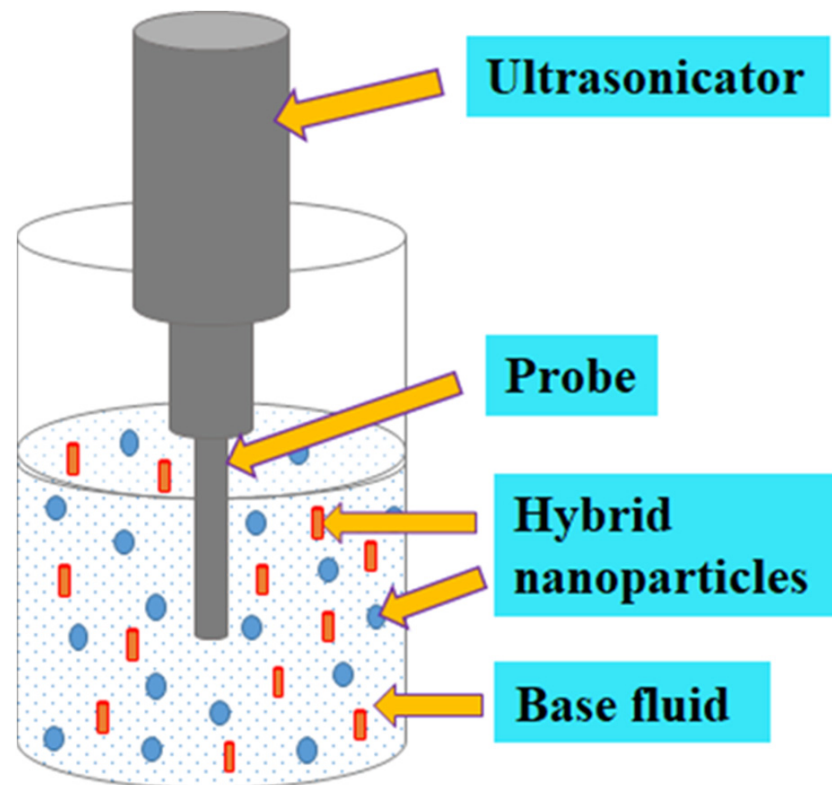


Figure 3. Ultrasonication of HNF.

Addition of Surfactants

Surfactants are complex chemical compounds that create an electrostatic repulsion to overcome magnetic attraction (for magnetic NPs) and Van der Waals interaction between NPs to avoid their sedimentation in the suspended base fluids [111]. The primary reason for surfactant use in NF formulation is to aid the stability of NPs in the base fluid [111]. Surfactants lower the interfacial tension between NPs and base fluid to enhance the stability of NFs. The use of surfactants promotes the stability of NFs by increasing the EDL between NPs. Surfactants such as cetyl trimethyl ammonium bromide (CTAB), sodium dodecyl sulphate (SDS), gum Arabic (GA), oleic acid (OA), polyvinyl pyrrolidone (PVP), nanospere AQ, dodecyl trimethyl ammonium bromide, sodium dodecylbenzene sulfonate (SDBS), and hexa decetyl trimethyl ammonium bromide have been used in the literature to stabilize MNFs and HNFs [73,95,104,112–115]. A list of some surfactants used in NF studies is given in Table 1. An increase in κ , zeta potential (ZP), surface tension, and the μ of MNFs and HNFs due to the use of surfactants has been reported [95,103,106,109]. However, the effectiveness of surfactants at >60 °C was reported to reduce due to weak bonds between surfactants and NPs, which, when finally broken, may lead to sedimentation and thus the instability of MNFs and HNFs [112]. Different surfactants have been used by various researchers to stabilize MNFs and HNFs formulated from diverse NPs and HNPs and suspended in different base fluids [13,18,73,78,109,116,117]. Therefore, it can be concluded that the stability of MNFs and HNFs based on the use of surfactants is dependent on the type and nature (magnetic or not) of NPs or HNPs, the base fluid type (ionic or non-ionic), and the type of surfactants used.

Control of pH

The stability of MNFs and HNFs can be improved by adjusting the pH. By suspending NPs into a base fluid, surface electric charges are produced on the resultant NF, which can be manipulated by altering the pH value. The surface electrostatic charges affect the stability of NF. An alteration of the pH value farther from the isoelectric point (IEP) enhances the NF stability. The pH of NF determines the IEP of the suspension, and this

can be altered to improve the stability to avoid sedimentation and agglomeration. The IEP of some NFs is provided in Table 2. Additionally, the surface electric charge can be determined using ZP. The ZP measures the repulsion between NPs and increases with a rise in the particles suspended in the base fluid [73,118]. A high ZP (absolute value) indicates the stability of NFs due to a strong electrostatic repulsion between NPs, while a low ZP shows instability due to the weak electrostatic repulsion of particles. With a ZP value of >60 mV, a very stable NF is formulated; a value of >30 mV implies a stable NF, whereas <20 mV indicates weakness in NF stability [73,96,103]. Zawrah et al. [73] reported the modification of the pH of Al₂O₃/water NF (with a surfactant of SDBS) from 5 to 10 using NaOH because the IEP of the NF was around 6.3. Similar pH alterations to improve NF stability were carried out in other studies [85,106,119–121]. The pH of MNFs and HNFs is given in Table 3.

Table 1. List of surfactants used in nanofluid studies.

Name
Sodium dodecyl sulphate
Sodium dodecylbenzene sulfonate
Gum Arabic
Oleic acid
Cetyl trimethyl ammonium bromide
Polyvinyl pyrrolidone
Nanosperse AQ
Dodecyl trimethyl ammonium bromide
Hexa decetyl trimethyl ammonium bromide
Sodium hexa meta phosphate
Span 80
eriochrome blackT
Triton X100
Tween 80
Citrus acid
3-Aminopropyl) trimethoxysilane
Polyisobutene succinimide
Sodium deoxycholate
Poly(vinyl alcohol)
Polyisobutene succinimide
Tetramethylammonium hydroxide

Table 2. Isoelectric points of mono and hybrid nanofluids.

Nanofluids	IEP	References
Al ₂ O ₃	9.1	Kumar and Sarkar [122]
Al ₂ O ₃	6.2–6.8	Zawrah et al. [73]
MgO	6.82	Kumar and Sarkar [122]
SiC	7.56	Kumar and Sarkar [122]
AlN	8.12	Kumar and Sarkar [122]
Cu	7.73	Kumar and Sarkar [122]
MWCNT	7.62	Kumar and Sarkar [122]
Al ₂ O ₃	8.0	Mahbubul et al. [123]
TiO ₂	6.5	Mahbubul et al. [124]
TiO ₂	2–4	Sreekumar et al. [125]
Sb ₂ O ₅	3–5	Sreekumar et al. [125]
Al ₂ O ₃	8.0	Cacua et al. [126]
TiO ₂	6.2	Chakraborty et al. [127]

Table 3. pH of mono and hybrid nanofluids.

Nanofluids	pH	References
Al ₂ O ₃ -TiO ₂ (8:2, 6:4, 4:6, 2:8)/DW	5.68–5.75	Kumar and Sarkar [122]
Al ₂ O ₃ + MgO/DW	8.23	Kumar and Sarkar [128]
Al ₂ O ₃ + SiC/DW	6.82	Kumar and Sarkar [128]
Al ₂ O ₃ + AlN/DW	7.56	Kumar and Sarkar [128]
Al ₂ O ₃ + Cu/DW	8.12	Kumar and Sarkar [128]
Al ₂ O ₃ + MWCNT/DW	7.73	Kumar and Sarkar [128]
Al ₂ O ₃ /DW	7.62	Kumar and Sarkar [128]
Al ₂ O ₃ /DW	8.0	Wang and Li [129]
Cu/DW	9.5	Wang et al. [106]
Cu-Al ₂ O ₃ /DW	5.5	Momin et al. [130]
SiO ₂ -CuO/C/GL-EG (60:40)	8–9	Akilu et al. [131]
SiO ₂ -GNP/naphthenic mineral oil	9–11	Qing et al. [132]
Fe ₃ O ₄ -GNP/DIW	3, 5, 7, 8, and 10	Askari et al. [101]
Al ₂ O ₃ and Al ₂ O ₃ -Fe (50:50)/DIW	12	Okonkwo et al. [133]
Al ₂ O ₃ /W	7–8.2	Menbari et al. [85]
CuO/W	8–9	Menbari et al. [85]
Al ₂ O ₃ -CuO/W	7.6–8.5	Menbari et al. [85]
Al ₂ O ₃ /EG	6.5–7.5	Menbari et al. [134]
CuO/EG-W (50:50)	8–9	Menbari et al. [134]
CuO/EG	8.5–10	Menbari et al. [134]
Al ₂ O ₃ /EG-W (50:50)	7–8	Menbari et al. [134]
Al ₂ O ₃ -CuO/EG	7–8.2	Menbari et al. [134]
Al ₂ O ₃ -CuO/EG-W (50:50)	7.2–8.5	Menbari et al. [134]
Al ₂ O ₃ -CuO/W	7.5–8.5	Menbari et al. [135]
Al ₂ O ₃ -CuO/EG-W	7–8.2	Menbari et al. [135]
Cu/DIW	7.43–10.2	Kamalgharibi et al. [86]
Cu/EG-DIW (50:50 vol)	7.8–9.6	Kamalgharibi et al. [86]
Cu/EG	9.85–10.2	Kamalgharibi et al. [86]
Al ₂ O ₃ /W	5.1–5.2 (sonicated) and 5.4 (without sonication)	Mahbulbul et al. [123]
MgO/EG	9.66–10.84	Adio et al. [120]
Al ₂ O ₃ (100 nm)/GL	4.09	Adio et al. [74]
Al ₂ O ₃ (80 nm)/GL	6.26	Adio et al. [74]
Al ₂ O ₃ (20–30 nm)/GL	6.44	Adio et al. [74]
Cu-TiO ₂	7	Sajid and Ali [92]
Al ₂ O ₃ -Cu	5.5	Sajid and Ali [92]
Ag-MgO	5.74	Sajid and Ali [92]
SiO ₂ -GNP	11	Sajid and Ali [92]
ZnO/W	4	Sajid and Ali [92]
Al ₂ O ₃ /BDW	10	Zawrah et al. [73]
TiO ₂	7	Chakraborty et al. [127]
Ag-TiO ₂	7.3–8.35 (without sonication) and 7.70–8.69 (sonication)	Chakraborty et al. [127]

Functionalization of Nanoparticles

The surface modification or functionalization of NPs is another technique employed to improve the stability of NFs. This stability-enhancing method is surfactant-free but needs materials for functionalization. Although this technique is not widely studied, it is a promising method for the formulation of more stable MNFs and HNFs [104,105,136]. Owing to the importance of the stability of MNFs and HNFs, the measurement of this parameter is key to the further use of MNFs and HNFs in terms of thermophysical properties and convective heat transfer studies.

2.3.3. Stability Test Methods

Visual Inspection

The simplest method to check the stability of MNFs and HNFs is by visual inspection. In other words, it is a visual observation of the MNF and HNF samples at daily or weekly,

or monthly intervals to see how the NPs or HNFs sediment with time. This is not a scientific method for checking the stability of MNFs and HNFs, as reported in the literature [74,104,137,138]. However, this method is always used in addition to other stability monitoring techniques that are scientific [74,104,109,137,138].

Zeta Potential

ZP is a method used to determine the stability of MNFs and HNFs. As earlier stated, the ZP of MNFs and HNFs is strongly connected to the repulsive force between the NPs or HNFs. This technique is mostly used to measure the stability of MNFs and HNFs, as reported in the literature by several authors [1,73,98,121,131]. The degree of stability of MNFs and HNFs can be determined using this method based on the obtained ZP values. It is worth mentioning that this stability-checking technique is often used along with other techniques.

Ultraviolet-Visible Spectrophotometer

This method seems to be the most employed of all the methods for monitoring the stability of MNFs and HNFs. The absorbance or transmittance of the MNFs and HNFs at the peak wavelength can be deployed to monitor the stability of MNFs and HNFs [20,79,85,109,139,140]. One distinguished merit of this method is the capability to check stability at regular intervals for a long time (days to months) [141], which other methods cannot offer. Thus, it provides an instantaneous measurement of the stability of MNFs and HNFs. Similar to other techniques, it is always used along with other methods such as visual inspection and ZP.

Checking of Thermophysical Properties

The stability of mono and hybrid NFs is also monitored by measuring their thermophysical properties over time. Garbadeen et al. [18] and Joubert et al. [20] monitored the stability of MWCNT/DIW and Fe₂O₃/DIW NFs for 250 min and 20 h, respectively, by measuring the μ . Likewise, in other studies, Yu et al. [142] and Ijam et al. [139] monitored the stability of Fe₃O₄/kerosene and GO/DIW-EG (60:40) NFs by measuring their κ for 360 min and 7 days, respectively. The use of κ to monitor the stability of NFs was corroborated by the work of Wang et al. [106], which reported a strong relationship between κ and the stability of NFs (Al₂O₃/W and Cu/W). Both Mahrood et al. [143] and Arani and Pourmoghadam [144] reported the use of density to monitor the stability of carboxymethyl cellulose-based Al₂O₃ and TiO₂ NFs (before and after) and EG-based Al₂O₃-MWCNT NF (five times in 14 days), respectively. Additionally, Babu and Rao [145] used turbidity to check the stability of water-based Al₂O₃ NF. The literature showed that two or more of these reported NF stability monitoring techniques were used to check the stability of mono and hybrid NFs.

3. Influence of Preparation Characteristics on Stability, Properties, and Performance

3.1. Mono NFs

3.1.1. Thermal Properties

The influence of sonication time (2.5–10 min) of DIW-based Fe₃O₄ (0.494–2.428 wt%) + CNT (0.105–1.535 wt%) NFs on κ was investigated [146]. GA and TMAH are used as surfactants to formulate the HNFs for this study. The result demonstrates that the maximum values (15.59% for 0.494% Fe₃O₄ + 0.105% CNT and 34.26% for 2.428% Fe₃O₄ + 1.535% CNT at 55 °C) of the κ are recorded when sonication is performed for 5 min. The influence of sonication time (2–8 h) on the stability, κ , μ , specific heat capacity (c_p), specific gravity, and pH of DIW-based ZnO and CuO NF (0.1 wt%) was examined [147]. Eriochrome Black T (EBT) is used as a surfactant for ZnO NF, while oylamine is used for formulating CuO and ZnO NF with 0.1 wt% concentration. The stability of the NFs is determined using visual inspection, ZP, and absorbency tests. For all the NFs, the ZP is observed to increase with sonication time, and the ZnO + EBT NF is found to be the most stable. The results

demonstrated that the sonication time did not affect the pH and specific gravity of the NFs, whereas the c_p , μ , and κ are affected by sonication time. The authors stressed the need to optimize c_p , μ , and κ as the stability of the NFs is affected by sonication time. Figures 4–6 show the effect of sonication time on the κ , μ , and ρ of MNF and HNF, respectively.

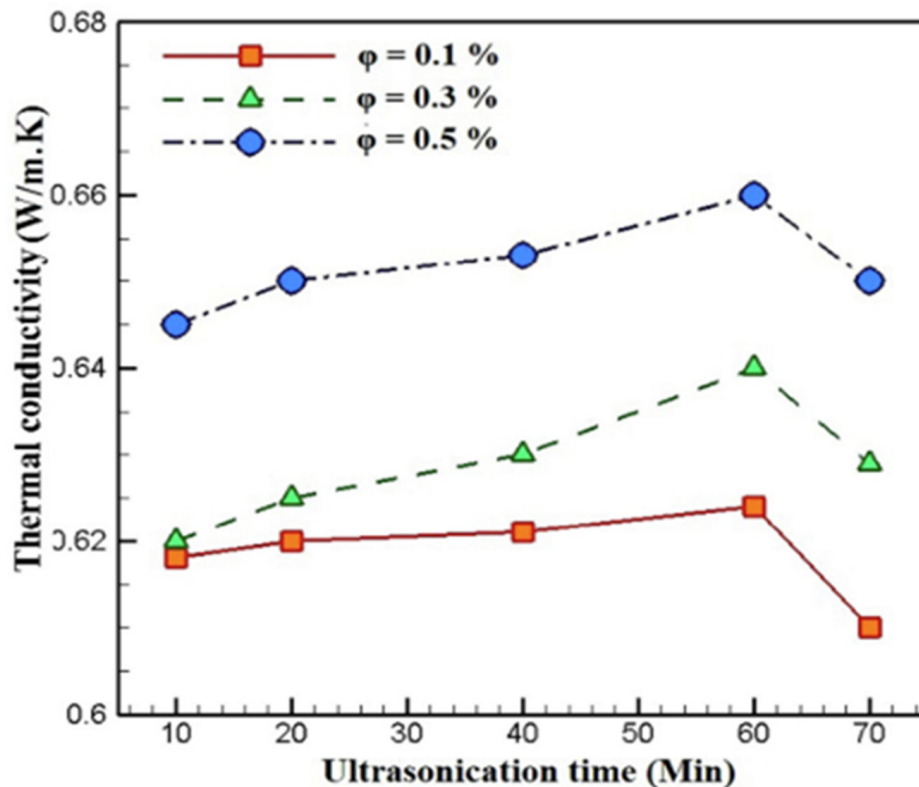


Figure 4. Thermal conductivity of MWCNT/water NF against ultrasonication time at the temperature of 35 °C and different concentrations. Adapted from [148].

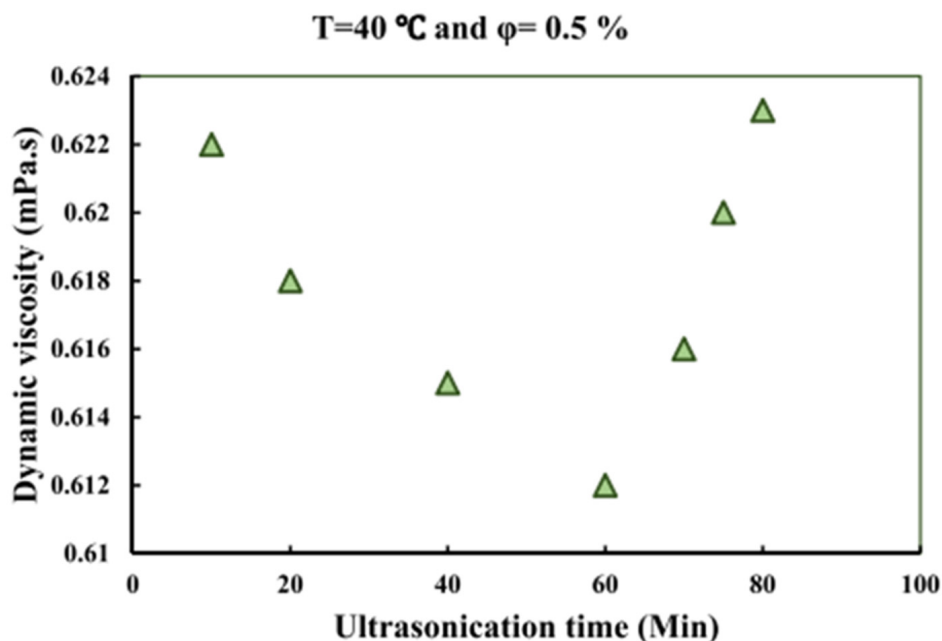


Figure 5. Viscosity of MWCNT/water NF against ultrasonication time at the temperature of 40 °C and concentration of 0.5%. Adapted from [149].

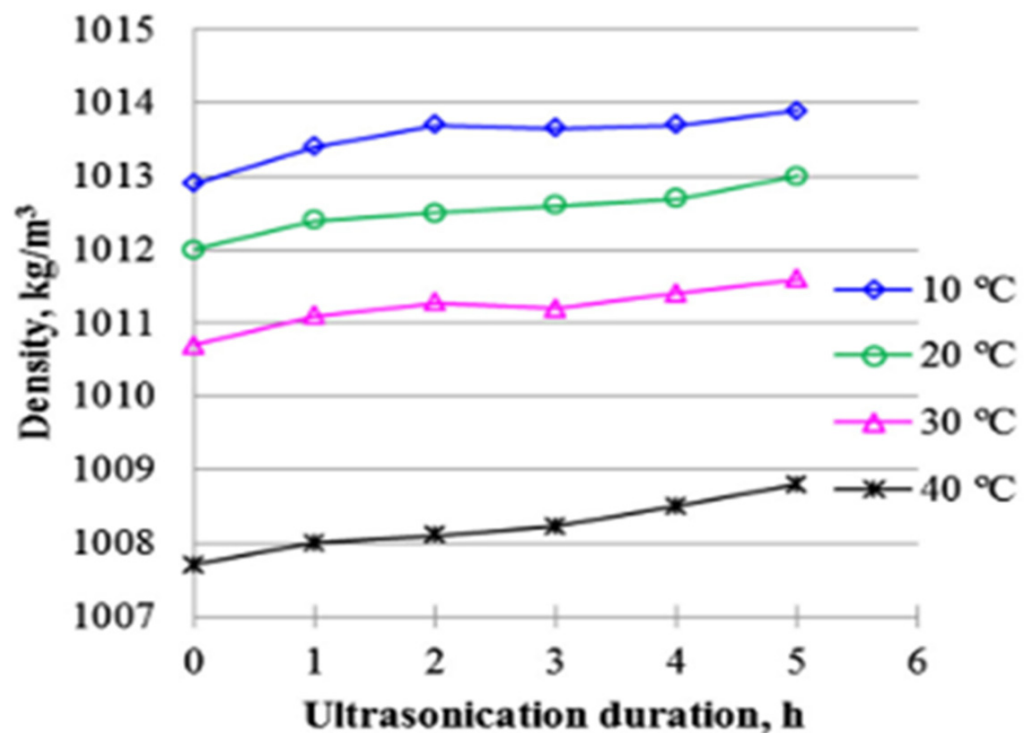


Figure 6. Influence of ultrasonication duration on density of 0.5 vol% Al_2O_3 -water NF at different temperatures. Adapted from [150].

The influence of sonication time (10–160 min) and surfactants (CTAB, OA, and SDS) on the stability and κ of $\text{Mg}(\text{OH})_2$ NFs (0.1–2 vol%) was examined [151]. Visual inspection and ZP are tests used to determine the stability of these NFs. It is observed that increasing the sonication time leads to a reduction in ZP and κ values. The NF prepared using CTAB as a surfactant and sonicated for 30 min is noticed to be the most stable with ZP of 53 mV (after 7 days) and 51 mV (after 30 days). The stability and κ of DW-based GNP NF (0.1 wt%) under different amounts of SDBS and SDS (1:3–3:1) were investigated [152]. The stability is checked using visual inspection, UV, and ZP. Results proved that the use of SDBS and SDS yields stable NFs (>30 mV), with SDBS exhibiting better stability than SDS, as indicated by the ZP and UV results. Moreover, the κ of SDS-based NF is higher than that of SDBS-based NF, with the maximum κ obtained using 0.05 g of SDS (2:1) in GNP NF.

The impact of sonication time (20–60 min) on the stability and κ of WO_3/EG NFs (0.005–5 wt%) was examined [153]. An increase in the sonication time is observed to enhance κ for all samples of the MNF, with the peak value obtained at 60 min of sonication. Very stable WO_3/EG NF is observed as indicated by ZP of 63.8 mV. Up to a 4% increase in κ is reported with a sonication time of 60 min. The response surface methodology scheme is used to optimize the influence of the amounts of MWCNT (0.01–1 w/v), Fe_2O_3 (0.1–2 w/v), pH (2–10), and volume of EG-W (30–70 v/v) on the κ of MWCNT- Fe_2O_3 NFs [138]. Maximum κ of 0.534 W/mK is obtained with optimal values of 0.69 w/v (MWCNT), 1.67 w/v (Fe_2O_3), 44 v/v (EG), and pH of 6.5. These optimal values also resulted in maximum σ , μ , and density (ρ) of 545 $\mu\text{s}/\text{cm}$, 1.2 g/ms, and 1174.6 kg/m^3 , respectively. The amount of MWCNT in the HNF is noticed to impact κ and other thermal properties the most. A correlation is proposed for the estimation of κ using the amounts of MWCNT and Fe_2O_3 , pH, and volume of EG-W (see Table 4).

Table 4. Correlations for the estimation of κ , zeta potential, and solar weighted absorption fraction of NFs based on various preparation characteristics.

Authors	Correlation	Remark
Asadikia et al. [154]	$\kappa = 0.42 - 0.028EG + 0.0168MWCNT + 0.007Fe_2O_3 - 0.02pH - 0.024MWCNT * EG + 0.021Fe_2O_3 * EG + 0.052pH * EG + 0.01MWCNT * Fe_2O_3 - 0.015MWCNT * pH - 0.015.Fe_2O_3 * pH$	Effect of EG, Fe ₂ O ₃ , MWCNT, and pH on κ (κ).
Mahbubul et al. [124]	$ZP = 10.742 + 0.013ACS - 0.308ST + 0.003ACS * ST$ $ZP = 34.021 - 0.06ACS + 0.096ST$	Effect of average cluster size and sonication time on ZP.
Sreekumar et al. [125]	$SWAF = 245.66 - 1049.47 * ATO.AG - 2499.67 * SMF + 18,926.22 * ATO.AG * SMF - 810.18 * (ATO.AG)^2 + 7961.97 * SMF^2 - 61,244.95 * ATO.AG * SMF^2$	Effect of ATO-AG and surfactant mass fraction (SMF) on solar weighted absorption fraction (SWAF).

The impact of sonication time (10–80 min) on the μ and stability of MWCNT/W NFs (0.1–0.5 vol%) was investigated [149]. The stability is monitored using the visual inspection, UV, and ZP methods. The results revealed that the ZP increases and μ reduces as the sonication time increases to 60 min, after which a reverse trend is observed. Therefore, stable MNFs and the lowest μ are achieved with 60 min of sonication. In addition, the ZP of the MNFs reduces as storage duration increases up to 30 days. A similar study to that of [149], except for the measurement of κ of MWCNT/W NF instead of μ , was conducted [148]. The κ is enhanced as the sonication time increases to 60 min, with a reduction observed as the sonication time further increases. At 60 min of sonication, optimal stability is achieved, as indicated by the highest ZP value and minimum sedimentation of the MNF after 30 days (visual indication).

The stability, κ , and μ characteristics of PVP + Al₂O₃/DW NFs under varying concentrations (0.5–2 vol%) and sonication times (30–150 min) were studied [83]. Results demonstrated that as the sonication time increases κ is enhanced while μ is reduced to the optimum point. A further increase in sonication time causes the κ to reduce while the μ is increased due to re-agglomeration. It is observed that the optimum sonication time increases as the volume concentration of Al₂O₃/DW NFs rise leading to a reduction in the average particle size. The sonication times of 60 min (0.5 and 1 vol%), 90 min (1.5 vol%), and 120 min (2 vol%) are recorded in this work, which contradicted the report of [148,149], which published an optimum sonication time for all the studied volume concentrations. With sonication time of 90 min and 120 min, maximum enhancement of κ is 14.6% and 16.1% for 1.5 vol% and 2 vol% Al₂O₃/DW NFs, respectively, while at 90 min of sonication μ is reduced by 33% (minimum) for 1.5 vol% Al₂O₃/DW NF. The effect of sonication time (0.5–5 h) on the stability, μ , κ , and ρ of 0.5 vol% Al₂O₃/DW NF was examined [150]. The studied sonication duration is equivalent to a sonication energy of 8460 (1 h), 16,920 (2 h), 25,380 (3 h), 33,840 (4 h), and 42,300 (5 h) J. By increasing the sonication time, ZP, κ and ρ are enhanced, while the cluster size and μ are reduced. Optimum stability conditions are reached at a sonication time of 5 h leading to optimal ZP (>55 mV), cluster size (105 nm), sonication energy (42.3 kJ), μ (1.63 mPa.s), κ , and ρ values. For 24 h and 30 days of storage of 0.5 vol% Al₂O₃/DW NF after sonicating for 5 h, the ZP values are observed to be similar. The influence of sonication time on the morphology of NF is presented in Figure 7.

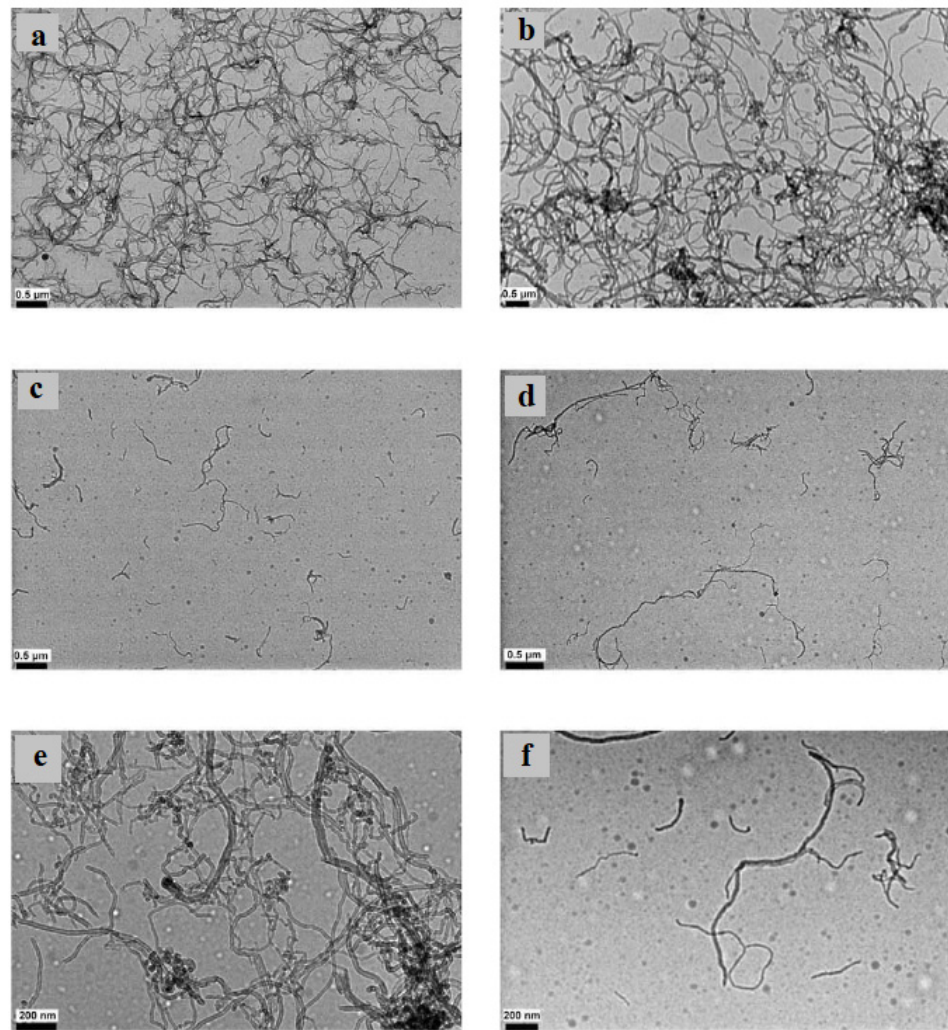


Figure 7. Images of Wet-TEM of 1 wt% MWCNT + 0.25 wt% GA NF sonicated for: (a) 20 min at 0.5 μm scale, (b) 40 min at 0.5 μm scale, (c) 60 min at 0.5 μm scale, (d) 80 min at 0.5 μm scale, (e) 40 min at 200 nm scale, and (f) 80 min at 200 nm scale. Adapted from [155].

The stability and κ behavior of various types of DW-based CNT NFs (SWCNT, DWCNT, FWCNT, and MWCNTs), formulated using three dispersion techniques (functionalization, bath/SDS, and probe/SDS), were studied [156]. Both the stability and κ of the resultant NFs depend on the dispersion techniques and NPs structure and size. The best stability and highest κ are achieved using the functionalized NFs due to their minimal agglomeration tendency and sedimentation, especially after 400 h. This is followed by probe/SDS and bath/SDS. An order of SWCNT > DWCNT > MWCNT (>10 nm) > MWCNT (10–20 nm) is observed for stability and κ of the NFs. The stability, μ , and κ of 0.1 wt% TiO₂/DW NF with and without SDS and horn ultrasonication or bath ultrasonication were examined [157]. The bath ultrasonication is carried out for 3 h while the horn ultrasonication lasted for 15 min. Results showed that the best stability (for 30 days) is achieved with the use of SDS and bath ultrasonication with ZP of 55 mV and particle size of 237.7 nm, followed by SDS and horn ultrasonication with ZP of 47.9 mV and particle size of 176.9 nm. However, the maximum values of μ and κ are achieved using SDS with bath and horn ultrasonication, respectively. Without SDS, the use of a sonication bath and horn resulted in relatively lower κ and μ associated with fair stability (ZP = 31.1–33.3 mV and particle size = 188.2–250.4 nm).

The influence of different surfactants (SDS and PVP), sonication time (0.25–2 h), nano-size (13 nm and 20 nm), NF concentrations (0.1–2.5 vol%), and surfactant mass fractions

(0.25–4 wt%) on the stability and κ of DIW-based $\alpha\text{Al}_2\text{O}_3$ NFs was studied [158]. The results demonstrate that the utilization of PVP to formulate the NF exhibits better stability than SDS even after 48 h of preparation. For both surfactants, κ reduces drastically, as the mass fraction increases up to 1.0 wt%, after which a relatively constant κ is noticed when the mass fraction of the surfactants is increased further. The κ of $\alpha\text{Al}_2\text{O}_3$ NF is observed to reduce after preparation, but it enhances with an increase in sonication time and volume concentration. After preparation, no significant difference in κ is observed for samples ultrasonicated for 1 h and 2 h. With the use of SDS and PVP, maximum κ is achieved at different optimum surfactant mass fractions for different volume concentrations, and the SDS is noticed to yield higher values of κ . The $\alpha\text{Al}_2\text{O}_3$ NF with a nano-size of 13 nm exhibited higher κ than the 20 nm-based NF with optimal κ values at 0.5 wt% and 1.0 wt% for SDS and PVP, respectively.

The stability and κ characteristics of $\gamma\text{Al}_2\text{O}_3$ /DIW NF under varying volume concentrations (1, 2, and 3 vol%) and sonication duration (15–180 min) were studied [159]. Depending on the volume concentration, polydispersity index (PI), absorbance, and cluster size decreases with an increasing sonication time, while ZP and κ are increased with a sonication time increase. At 150 min of sonication, peak κ and ZP (>50 mV), constant absorbance, and minimum cluster size and PI are achieved. An increase in the volume concentration resulted in an increase in κ , cluster size, and PI, and a reduction in the absorbance after 30 min of sonication. The impact of the sonication time (5–30 min) and energy density (2.4×10^5 – 1.4×10^6 kJ/m³), and surfactant concentration (0.3–8 wt%) on the aspect ratio, κ , flow behavior, and μ of 0.12 vol% MWCNT/W NF was examined [160]. Using 5 min of sonication (corresponding to 2.4×10^6 kJ/m³), the lowest value of μ and κ are achieved at an optimum surfactant concentration of 3 wt%. The NF exhibits a Newtonian behavior under increasing stress at the optimum surfactant concentration. An increase in the sonication time (and corresponding energy density) is observed to cause a reduction of μ (with increasing stress), κ , and aspect ratio. Therefore, the optimum sonication time to achieve a stable 0.12 vol% MWCNT/W NF is 30 min.

The influence of sonication time (4–100 h) on the κ , nanoparticle cluster size, and stability of ZnO/EG NF (0.5–3.75 vol%) was studied [161]. Increasing the sonication time from 4 h to 60 h results in a decrease in nanoparticle cluster size (459–91 nm) and an increase of κ (21–40%), in which the reverse is observed after a further increase in the sonication time. This implies an improvement of the stability of ZnO/EG NF as the sonication time increased to 60 h through a nanoparticle cluster size reduction leading to the enhancement of κ . After 60 h, the cluster size of the NF increases, leading to the instability and reduction of κ . Using the optimum sonication time of 60 h, a relatively constant κ is observed with no sedimentation for 30 days after preparing 1 vol% ZnO/EG NF. The stability of MWCNT/DW NF under varying sonication times (5–120 min), weight concentrations (0.1–1.5 wt%), and SDS concentrations (0.01–0.4 wt%) was reported [162]. The results demonstrate an optimum stability condition at an optimum sonication time of 90 min (1×10^5 J) and an SDS concentration of 1.5 wt% for MWCNT/DW NF with a weight concentration of 0.1–1.4 wt%, as indicated by the constant values of their absorbance. It is observed that increasing the SDS concentration causes an increase in the sonication energy required to formulate the MWCNT/DW NF.

The influence of sonication time (5–1355 min) on the κ , μ , shear stress, average cluster size, and CNT length of 0.5 wt% MWCNT/EG + 0.25 wt% GA NF were studied [163]. Increasing the sonication time causes the reduction of μ , average cluster size, and CNT length and an increase in κ of the NF. At 1355 min of sonication, maximum κ (23%), minimum μ , lowest average cluster size, and CNT length are recorded owing to optimum stability conditions. The use of the continuous mode of sonication is observed to produce a slightly higher κ than the pulse mode. Figure 8 shows the impact of μ on the shear rate at different sonication times. The influence of aggregate size, sonication time, and temperature on the stability and μ of EG-based Cu NF was examined [164]. Stirring is carried out for 20 min, while sonication took 15–75 min at temperatures of 20–50 °C. Generally, a sonication

time increase causes a reduction in the μ value of the MNF, which enhances with a further increase in the sonication time after reaching the lowest μ , while a sonication temperature increase lowers the viscosity of the MNF. Increasing the sonication temperature and time is found to reduce the aggregate size of the NF due to an increase in Brownian motion. At low weight concentrations (1 and 2 wt%), the lowest μ values are obtained at an optimum sonication time of 60 min. However, for 3.8 wt% NF, the lowest μ is attained at an optimum sonication time of 45 min.

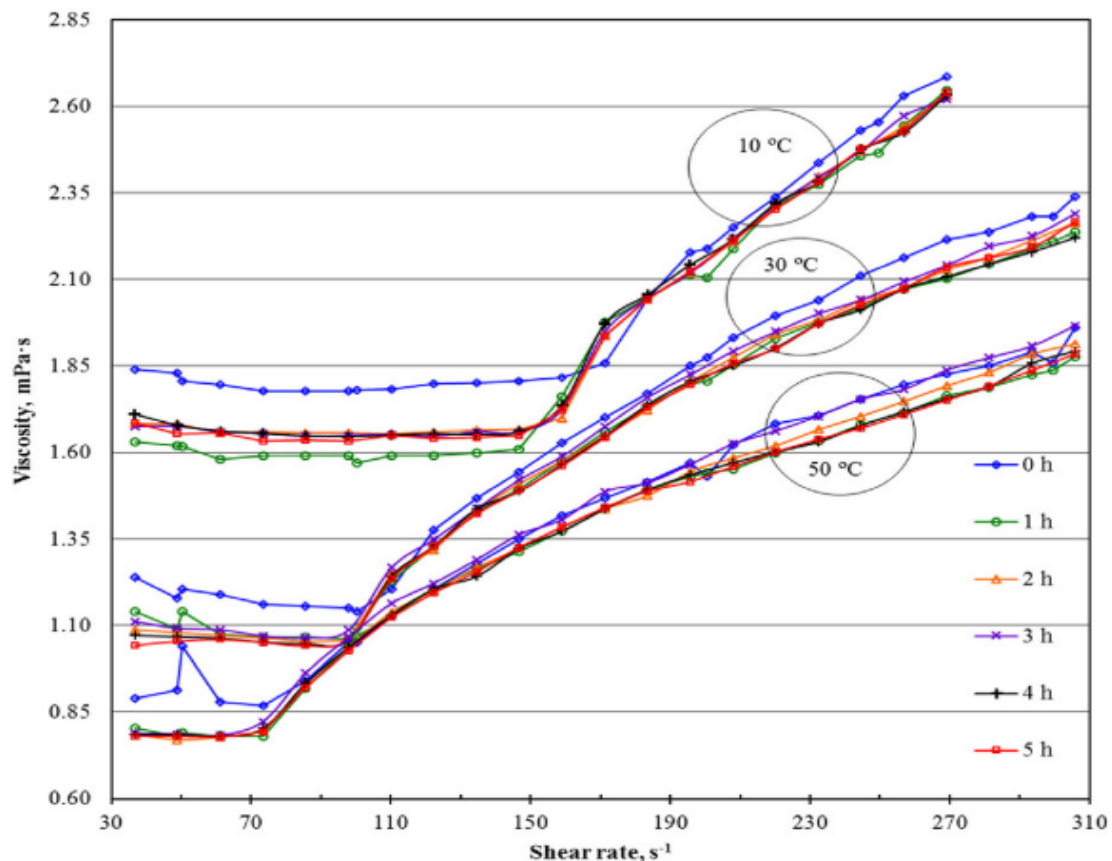


Figure 8. Viscosity against shear rate of Al_2O_3 NF at different sonication time. Adapted from [165].

The μ behavior of $\text{Al}_2\text{O}_3/\text{GL}$ NFs under different volume fractions (1–5%), sonication energy densities (5×10^6 – 4×10^7 kJ/m^3), nano-sizes (20–30, 80, and 100 nm), and sonication time (1–8 h) was investigated [74]. The stability is monitored using UV, ZP, and visual inspection techniques. The results demonstrate that the μ of $\text{Al}_2\text{O}_3/\text{GL}$ NFs reduces with the sonication time (irrespective of volume fraction) to an optimal value and thereafter increases as the sonication time increases. Stable $\text{Al}_2\text{O}_3/\text{GL}$ NFs are achieved by sonicating 20–30 nm-sized $\text{Al}_2\text{O}_3/\text{GL}$ NFs for 6 h and 80 nm and 100 nm-sized $\text{Al}_2\text{O}_3/\text{GL}$ NFs for 3 h. The sonication time of Al_2O_3 (20–30 nm)/GL NFs corresponds to the energy density of 3×10^7 kJ/m^3 , while that of Al_2O_3 (80 and 100 nm)/GL NFs amounts to 1.5×10^7 kJ/m^3 . An increase in the sonication energy density is noticed to cause a significant reduction in the average particle size. At optimum stable conditions, the MNFs have a pH, ZP, and particle size of 6.44, -504 mV, and 59.6 nm, 6.26, -244 mV, and 128.7 nm, and 4.09, -79 mV, and 118.0 nm for 20–30 nm, 80 nm, and 100 nm-sized $\text{Al}_2\text{O}_3/\text{GL}$ NFs, respectively. Moreover, at the optimum stability state, the Al_2O_3 (20–30 nm)/GL NFs are observed to exhibit the highest μ leading to a higher sonication energy density. Figure 9 presents the effect of sonication time on the viscosity of MNFs with different nano-sizes.

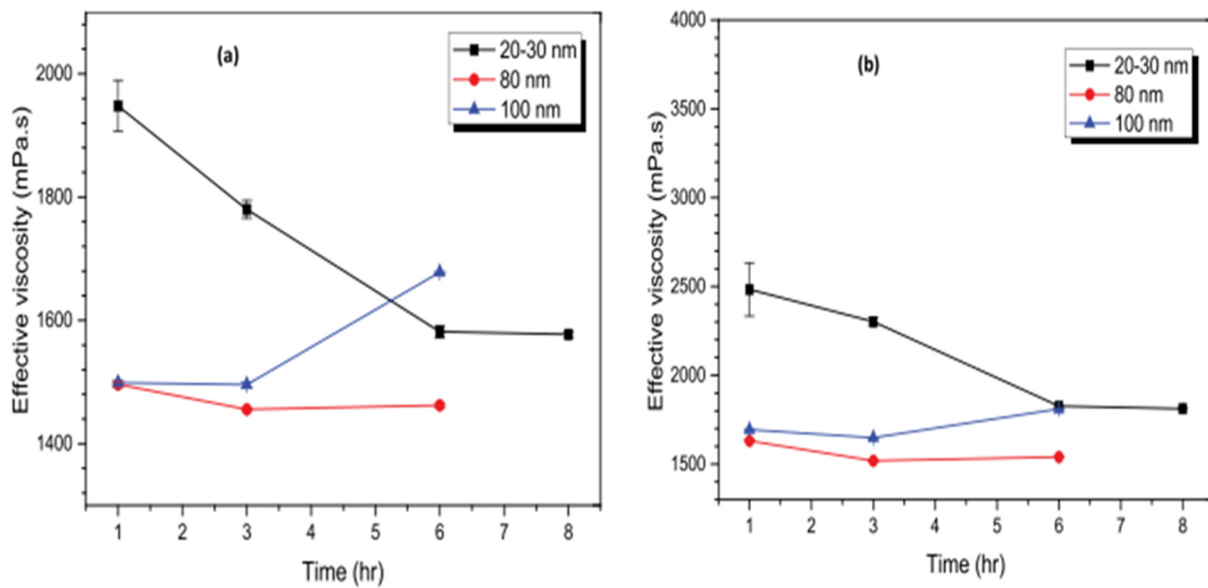


Figure 9. Influence of sonication time on viscosity of Al₂O₃-GL NF with volume fractions of (a) 2% and (b) 3%. Adapted from [98].

The stability and μ characteristics of MgO/EG NFs under different volume fractions (0.1–5%), nano-sizes (21, 105, and 125 nm), and sonication energy density were examined [98]. The optimal stability of the MgO/EG NFs is reached using a sonication energy density of 2.2×10^6 (30 min), 4.4×10^6 (60 min), and 13×10^6 kJ/m³ (180 min) for 21, 105, and 125 nm-sized MgO/EG NFs, respectively. The 21 nm-sized MgO/EG NFs are observed to exhibit the highest μ and pH, followed by 105 nm and 125 nm MgO/EG NFs. The stability of the MgO/EG NFs is reflected by a ZP of 38.5 mV (21 nm), 46.5 (105 nm), and 30.3 mV (125 nm). Increasing the sonication energy density is noticed to reduce μ of MgO/EG NFs in the order of 21 nm > 105 nm > 125 nm. The impact of sonication time (30–180 min) and nano-size (20 and 100 nm) on the stability, pH, and electrical conductivity (σ) characteristics of MgO/EG NFs was experimented with [120]. An optimal sonication time of 60 min (4.4×10^6 kJ/m³) is employed to obtain the stability of MgO/EG NFs with a 20 nm-based NF possessing a higher pH (9.66–10.84) and ZP (47 mV). The MgO/EG NFs with a nano-size of 100 nm are observed to exhibit a higher value of σ than the 20 nm counterpart. Figure 10 provides the σ of different concentrations of NF under varying sonication times.

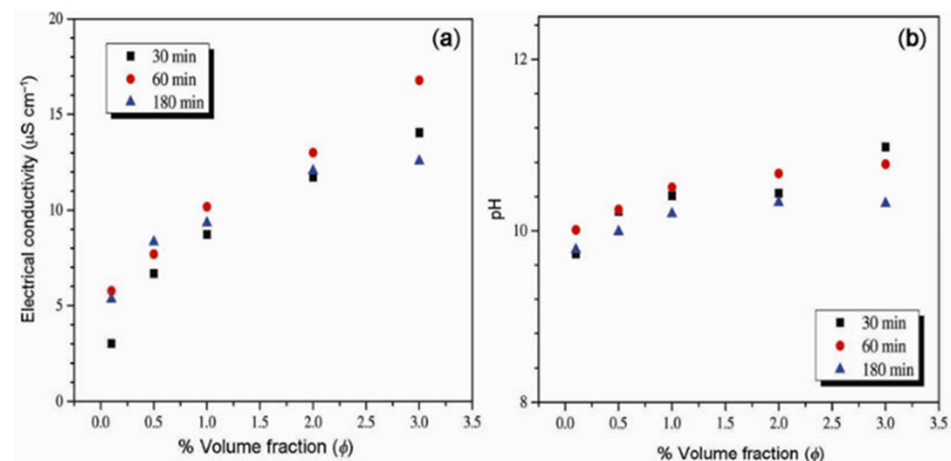


Figure 10. Influence of sonication time on the electrical conductivity and pH of MgO-EG NF at 20 °C: (a) electrical conductivity and (b) pH. Adapted from [120].

The stability via sedimentation and κ of MWCNT/EG NFs under the influence of sonication time (1–24 h) and volume fraction (0.05–2.5%) was examined [166]. An increase in the sonication time is observed to enhance the stability of the MWCNT/EG NFs as the particle size becomes smaller and the dispersion of nanoparticles improves. The settling time of the MNFs is noticed to increase as the volume fraction increases. The κ of the MNF enhances as the sonication time and volume fraction increase. The impact of sonication time (0–180 min) on the stability and μ of 0.5 wt% Al₂O₃/DIW NF was studied [167]. The results prove that an increase in the sonication time from 30 to 60 min causes an enhancement in μ , which diminishes as the sonication time is increased to 180 min. The ZP is noticed to increase as the sonication time increases, while the reverse is the case for the average cluster size and particle size. This reveals that the stability of 0.5 wt% Al₂O₃/DIW NF is enhanced with an increasing sonication time. The stability and rheological behavior of 0.5 wt% Al₂O₃/DIW NF under an increasing shear rate (36.7–305.7 s⁻¹) and sonication (1–5 h) were examined [165]. They demonstrated that the stability improvement and reduced μ are noticed with an increase in the sonication time. A Newtonian behavior is observed at lower shear rates (36.7–170 s⁻¹) depending on the temperature. With an increase in the sonication time, consistency indices of the MNF reduce slightly, while no specific trend is observed for the flow behavior indices.

Using the same sample and experimental setup as [165,168] studied the effect of sonication time (0–5 h) on the yield stress and behavior of 0.5 wt% Al₂O₃/DIW NF under an increasing shear rate (12.2–305.8 s⁻¹) using the Herschel–Bulkley model. A rapid reduction in yield stress is observed at the beginning of sonication (0–2 h), which reduced slowly from 2 h to 5 h of sonication (see Figure 11). The 0.5 wt% Al₂O₃/DIW NF is found to display a non-Newtonian behavior. With a slight reduction in yield stress at the start of the sonication, no noticeable difference is observed in the yield stress after a prolonged sonication. The flow consistency index is found to increase as sonication time increases, while no specific trend is observed for the flow behavior index under an increasing sonication. The effect of sonication time (1–5 h) on the stability, κ , μ , volume concentration, and storage of Al₂O₃/W NF at 0.5 vol% was examined [123]. The stability of the MNF is monitored by measuring ρ and used to evaluate volume concentration. It is observed that the sedimentation of the NP is reduced as the sonication time increases, leading to a stability improvement and storage of the NF. Moreover, the volume concentration, κ , and μ of the MNF reduces with the storage period but increase with the sonication time. The need to monitor the stability of NFs using ρ and κ and the enhancement of the thermal performance of NFs as the sonication time increases has been emphasized. In addition, the sonication time is observed to have a larger impact on μ than κ . In Figure 12, the stability of MNFs prepared at different sonication times is provided.

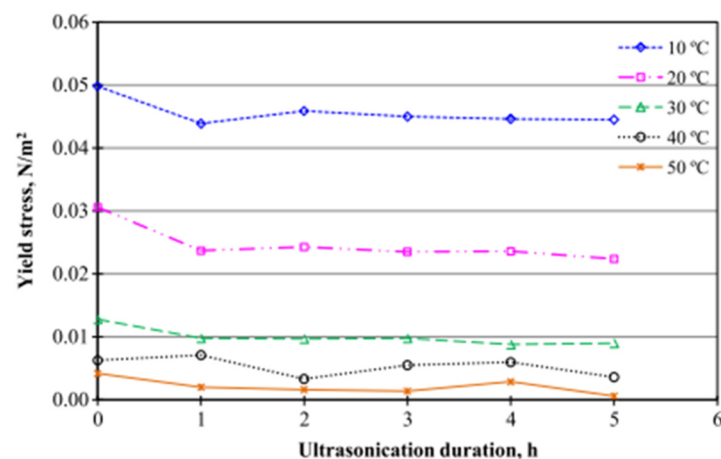


Figure 11. Effect of ultrasonication duration on the yield stress of the Al₂O₃-water NF. Adapted from [168].

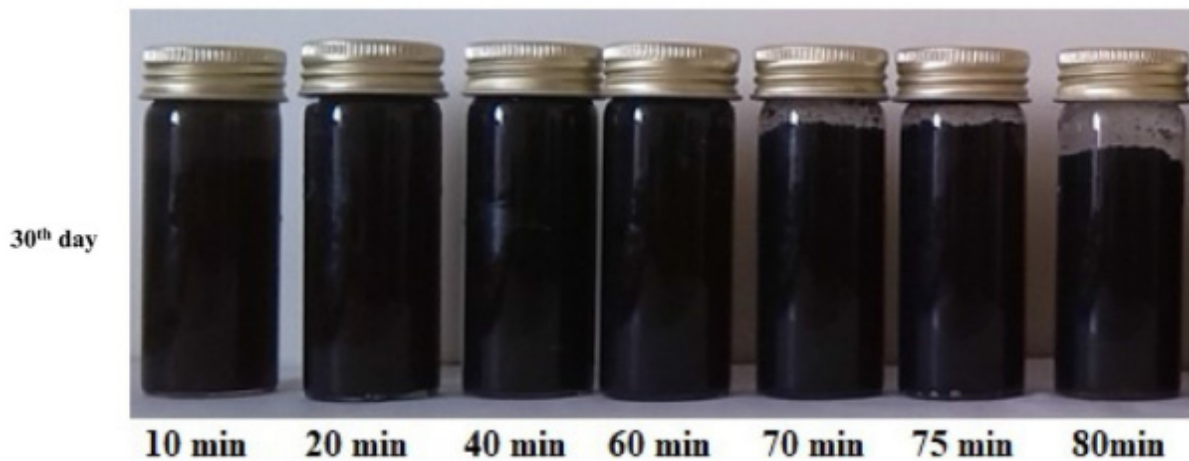


Figure 12. Stability of MWCNT-water NFs formulated at different ultrasonication durations (30 days). Adapted from [136].

The influence of φ (0.05–0.3 vol%) and sonication time (20–200 min) on the thermal properties (σ , C_p , θ , and κ) of f-MWCNT/DIW NFs was studied [169]. At 80 min of sonication, the 0.1 vol% sample has the highest long-term stability with 39.8 mV. A different optimum sonication time is observed for the thermal properties with 20 min (0.1 vol%), 20 min (0.3 vol%), 120 min (0.1 vol%), and 120 min (0.1 vol%) for κ , C_p , θ , and σ , respectively. A study on the influence of surfactant quantity, volume concentration, and sonication duration (5–30 min) on the stability, dispersion, wettability, and viscosity of oil-based MWCNT NFs was conducted [170]. The results demonstrate the use of a high sonication time (30 min), low surfactant quantity (1:10), and moderate concentration (0.4 vol%) to achieve optimum stability, dispersion, wettability, and viscosity. Two valid theories are proposed—contact line pinning and liquid nano-layering—to describe the role of nanoparticles in enhancing the contact angle of NF.

The impact of sonication times (0–4 h), φ (0.01–0.2%), and temperatures (30–45 °C) on the viscosity of Al₂O₃/DIW-EG (50:50 vol) NF was investigated [171]. An optimum sonication time of 3 h is achieved for all the studied concentrations with a maximum reduction of viscosity (11.36%) for the 0.2 vol% at 45 °C. The impact order of φ > temperature > sonication time was observed for the viscosity. An investigation of the influence of the sonication power (60–120 W), surfactant fraction (1:10–4:10), sonication (15–60 min), and stirring time 5–20 min of 0.24 vol% TiO₂/DIW NF at a sonication frequency of 20 kHz on κ and ZP as stability indicator was carried out [172]. To achieve maximum κ and stability of the NF, stirring time, sonication time, surfactant fraction, and sonication power of 15 min, 60 min, 2:10, and 120 W, respectively, are recorded. The contribution order of surfactant fraction > sonication power > sonication time > stirring time on κ is observed, while that on stability is surfactant fraction > sonication time > sonication power > stirring time.

3.1.2. Zeta Potential

The impact of the sonication time (5–30 h) on the stability characteristics of 0.1 vol% Al₂O₃/DIW NF using the ZP technique was investigated [173]. An optimum stability is reached at a sonication time of 5 h with a maximum ZP of 34 mV. The influence of pH on the stability of 0.1 wt% Al₂O₃/DIW NF under varying surfactant concentrations (0.5-critical micelle concentration (CMC) and 1-CMC) and surfactants (SDBS and CTAB) was examined [126]. Techniques of UV, ZP, average particle size, and visual inspection are used to check the stability of the NF with and without surfactants. The 1-CMC-SDBS Al₂O₃/DIW NF is observed to be most stable with a ZP of below 30 mV, pH of below 6, an average particle size of 123 nm, and a polydispersity index of under 0.3. Moreover, the absorbance of the NF is noticed to reduce as the time (20 days) increases, with 1-CMC-SDBS Al₂O₃/DIW NF recording the highest value. Under varying sonication amplitudes

(20–80%) and a sonication time of 30 min, the stability of the capped and bare Cu/methanol NF with 0.1% wt/vol concentration was studied [174]. The amplitudes correspond to energy and power densities of $0.07\text{--}0.42\text{ Wcm}^{-3}$ and $5\text{--}32\text{ Wcm}^{-2}$, respectively, while the ZP, average cluster size, and PI are used in relation to the stability of the MNFs. Increasing the sonication amplitude from 20% to 80% reveals an increase in stability, as indicated by an average cluster size (from 330 nm to 190 nm) and PI (from 0.229 to 0.162) reduction. The capped Cu/methanol NF is found to be more stable than the bare counterpart with ZP of 38 mV (for six months of storage), PI (<0.2), and average cluster size ($<200\text{ nm}$). Beyond the optimum sonication amplitude of 80%, a significant loss of methanol is observed due to the energy generated through sonication. The effect of sonication time on the ZP of MNFs, indicating the degree of stability and duration after preparation, is presented in Figures 13 and 14, respectively.

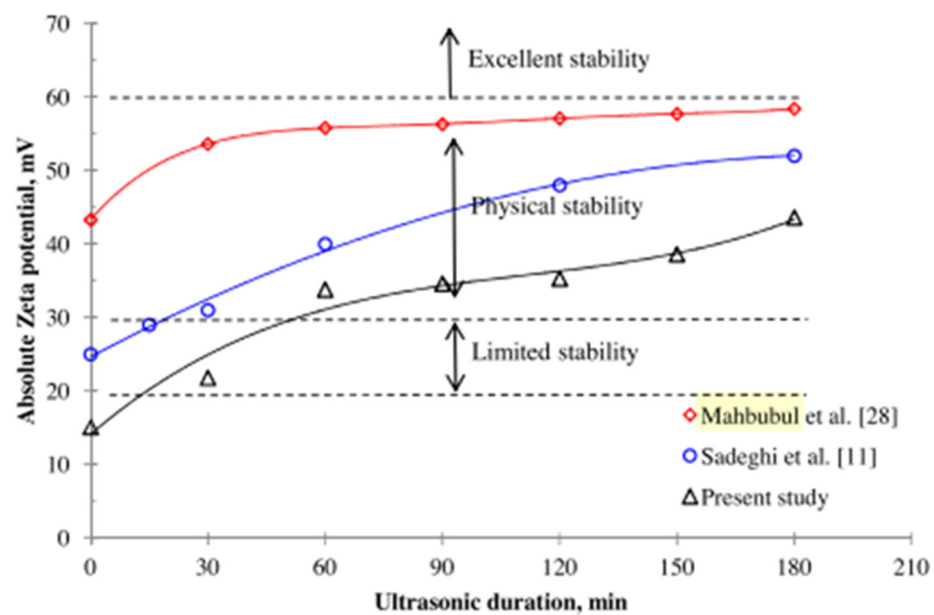


Figure 13. Effect of ultrasonic duration on zeta potentials of $\text{TiO}_2\text{--H}_2\text{O}$ NF. Adapted from [124].

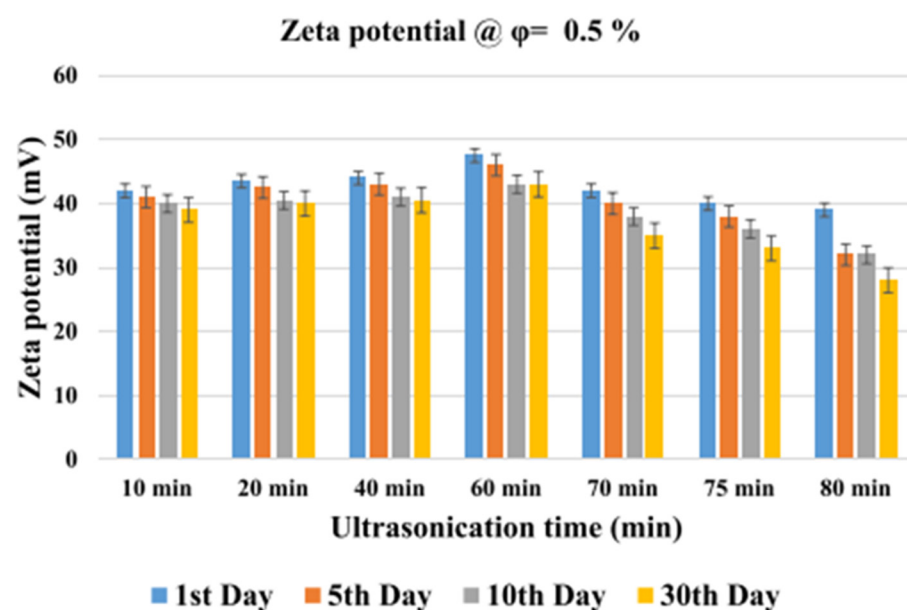


Figure 14. Effect of ultrasonication time on zeta potential of 0.5 vol% MWCNT/water NF at different storage time. Adapted from [148].

The stability and pH of water-based TiO₂ NFs (0.1 wt%) subject to the addition of Ag nanoparticles (0.1–0.4 wt%) and sonication time (10–30 min) were studied [127]. The sonication is found to be significant at ≤0.2 wt% of Ag NPs and 10 min of sonication beyond, which it is ineffective. The addition of the Ag particles and a sonication of the mixture is observed to increase the pH of Ag-TiO₂ NFs.

3.1.3. Absorbance

The stability of 0.025 w/v% SWCNT/DIW NF under varying sonication time (10–120 min) and power (20–120 W) using 3-mm and 6-mm tips for probe sonicator and centrifuge sonicator was studied [175]. Increasing the sonication power and time is observed to enhance the stability via the absorbent test. Optimum sonication power and time of 120 W and 120 min are attained, respectively. The use of a 6 mm tip for sonication is observed to yield better stability compared to that of a 3 mm tip sonicator (see Figure 15).

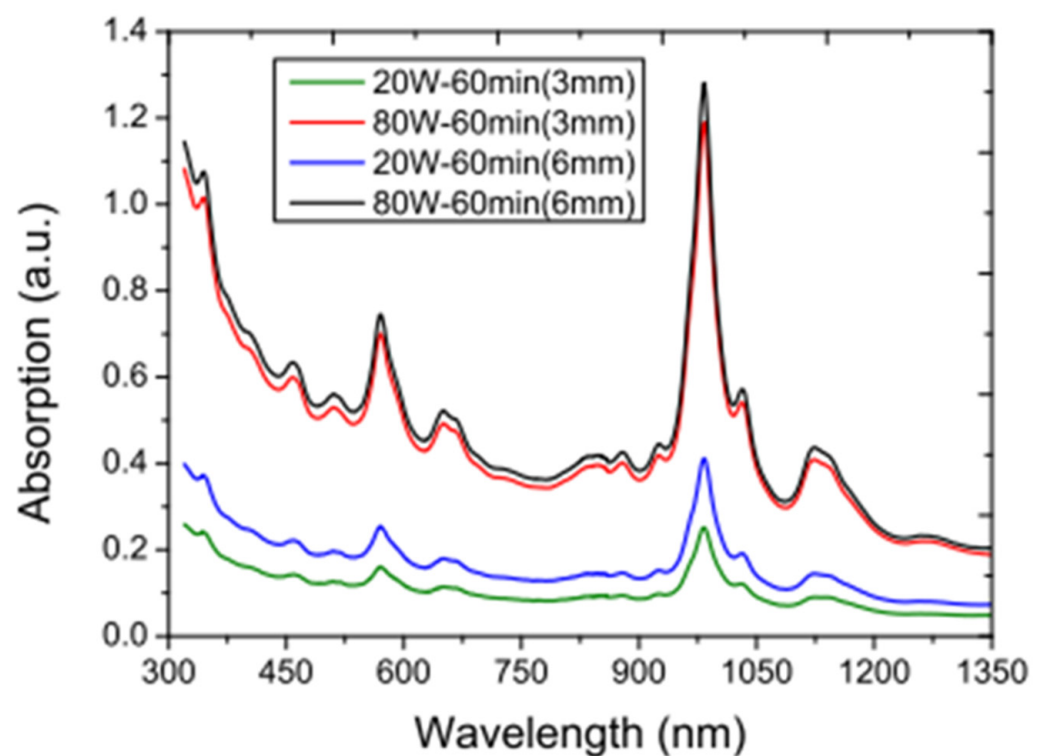


Figure 15. Comparison of the absorption spectra for the SWCNT NF dispersed using 3-mm and 6-mm sonication tips. Adapted from [175].

3.1.4. Surface Tension

Recently, the influence of sonication amplitude (40% and 100%), sonication time (0.5–4 min), and volume concentration (0.05–0.4 vol%) on the surface tension of ZnO/DW NFs were examined [176]. The following two parameters are considered: surface tension and relative surface tension of NFs. Owing to statistical analysis, sonication amplitude is noticed to have a significant difference in both parameters, while sonication time has a pronounced effect on the relative surface tension, while volume concentration has a significant difference on the surface tension (see Figure 16).

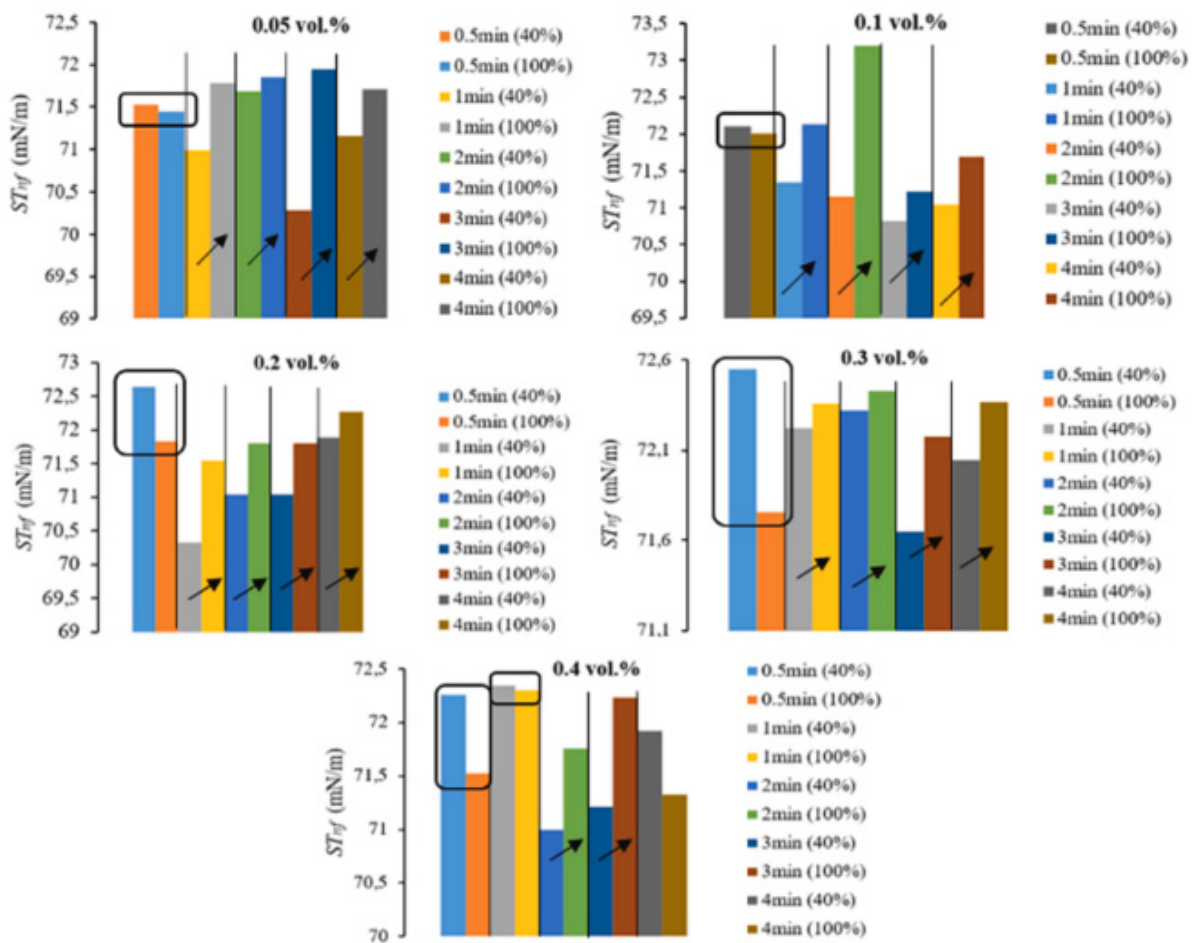


Figure 16. Effects of sonication amplitude (% in the parentheses) and time on ST_{nf} of ZnO/DW NFs. Adapted from [176].

3.1.5. pH

The Taguchi method was used to design and optimize the stability of Fe_3O_4 /DW NF in the absence and the presence of a magnetic field [87]. The parameters optimized are stirring speed (400–800 rpm) and time (30–90 min), surfactant mass (1–4) and types (citric acid, GA, Tween 20, SDS, and CTAB), pH (7–11), initial sonication (20–60 min), and final sonication time (0–40 min). The optimum parameters are reported using citric acid (surfactant), 600 rpm (stirring rate), 20 min (final sonication), 2% (surface mass), 11 (pH), 60 min (stir time), and 60 min (initial sonication) for the stability of Fe_3O_4 /DW NF without magnetic influence. However, the optimum parameters of 800 rpm (stirring rate), acetic acid (surfactant), 0 min (final sonication), 1% (surface mass), 10 (pH), 20 or 40 min (initial sonication), and 30 min (stir time) for the NF stability under the magnetic influence. The stability and pH of TiO_2 /DW NF (at 0.5 vol%), as measured by the ZP and average cluster size under varying sonication times of 0–180 min, were investigated [124]. It is observed that as sonication time increases, the pH and average cluster size reduces, but the ZP increases. However, at an optimum sonication time of 150 min (ZP = 38.6 mV and average cluster size = 139.4 nm), the best stability is observed. They developed a correlation to estimate the ZP of TiO_2 /DW NF from the average cluster size and sonication time.

The influence of the pH and SDBS (0–0.15 wt%) on the stability and κ for the aqueous Al_2O_3 and Cu NFs (0.05–0.8 wt%) was examined [106]. The stability is checked using the ZP. The results demonstrate that for Al_2O_3 and Cu NFs, the optimal pH, maximum ZP, optimal SDBS weight fraction, and minimum particle size values are ≈ 8 and ≈ 9.5 , 40:1 mV and 43:8 mV, 0.1 wt% and 0.07 wt%, and 240 nm and 310 nm, respectively. Moreover, maximum

κ (18% for Cu/W NF and 15% for Al₂O₃ NF at 0.8 wt%) is observed at the optimal SDBS and pH values. The optimum stability is observed at the optimal pH, ZP, and SDBS weight fraction values. This work and results are similar to that of [177], except for the weight fraction, the SDBS concentration, and the κ enhancement differences. The stability and κ of aqueous Cu and Al₂O₃ NF (0.01–0.4 wt%) under varying pH and SDBS concentrations (0–0.14 wt%). At 0.4 wt%, Cu and Al₂O₃ NFs are enhanced by 11% and 13%, respectively were studied [177].

In another study, the authors of [129] reported similar optimal pH values to that of [106] for water-based Al₂O₃ and Cu NFs (0.01–0.04 wt%). At these optimal values, the μ and κ of the MNFs are at a minimum and maximum value, respectively. Peak κ enhancement of 13% and 15% and μ of 0.825–0.865 and 0.2–0.86 mPa.s are recorded for Al₂O₃ and Cu NFs, respectively. At the optimal pH values, the optimum stability of the MNFs is noticed. Figure 17 shows the effect of sonication time on the pH of NF.

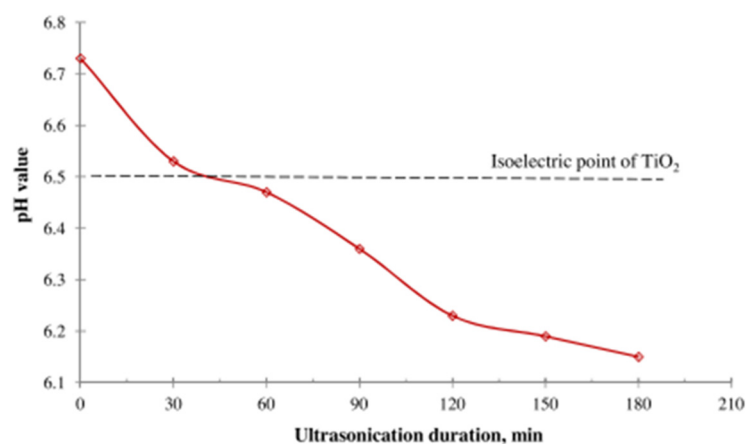


Figure 17. Influence of ultrasonication duration on pH value of TiO₂-H₂O NF with an isoelectric point of TiO₂. Adapted from [124].

3.1.6. Aggregate Size, Sedimentation Time, and Velocity

Nanoparticles in NFs aggregate as the distance between nanoparticles becomes lesser during the collision as the weak force of attraction (van der Waals) increases [178]. At high nanoparticle concentrations, the possibility of nanoparticle aggregation becomes high. The aggregation of nanoparticles in NFs is reported to enhance NF κ . This is connected to the localized particle-rich portion development with a lower thermal resistance to heat transfer compared to the less-particle portion. The formation of larger particle-free sections in the NFs leads to the settling of heavier aggregates (NF instability), which, consequently, reduces the κ and lowers heat transfer. NF stability is related to the aggregation characteristics, which can be determined by nanoparticle size and shape and the interaction energy between nanoparticles and base fluid.

Nanoparticles aggregate due to the force of attraction between the nanoparticles. The stability of CuO NFs (0.1–0.4 wt%) via the sedimentation height under different base fluids (DIW, EG-DIW (50:50 vol%), and EG), stirring rates (400–700 rpm), stirring time (60–75 min), surfactants (PVP, SDS, and Triton X100), sonication time (60–270 min), and sonication frequency (18–24 kHz) was studied [86]. The results show that EG and SDS are the best base fluid and surfactant, respectively, for formulating CuO NF. Increasing the stirring rate of CuO NF causes a reduction in the sedimentation height, but the optimum values are reported for the stirring and sonication time to achieve the lowest sedimentation height. The most stable NF (CuO/EG + SDS (1% volume of NF)) is achieved at a pH of 10.1, sonication time of 75 min, and stirring time of 60 min for 75 days.

Under changing sonication times (30–180 s), amplitudes (10, 30, and 60%), and irradiation methods (pulsed (0.1/0.1 and 1.0/1.0) and continuous (30 s and 90 s)), the stability characteristics of 1 mg/mL Al₂O₃/W NF through the cluster size was examined [179].

The most stable NF is observed to be formulated using an amplitude of 30%, sonication time of 180 s, and pulsed mode of 0.1/0.1 with a cluster size of <145 nm. They reported a slight difference in the cluster size using continuous and pulsed modes. Figure 18 presents the impact of sonication time on NP cluster size under different amplitudes. It is worth mentioning that nanoparticle shapes have been studied to affect the κ of corresponding NFs, while no significant effect is reported for the viscosity of NFs [169,171]. A higher aspect ratio, which is strongly connected to the surface area to volume ratio of nanoparticle shapes, has been attributed to the improvement in κ and consequently influences the heat transfer of NFs. However, the studies relating preparation characteristics to nanoparticle shapes are lacking in the public domain. The influence of different shapes (brick, blade, and platelets) of boehmite- Al_2O_3 particles on the stability and κ of boehmite- Al_2O_3 /water NFs was studied [180]. The NF stability was observed to be directly related to the nanoparticle shape, which consequently affects κ . NF with the brick-shaped nanoparticles has the best stability, followed by the platelets and blade-shaped nanoparticles. A similar trend was noticed for the κ .

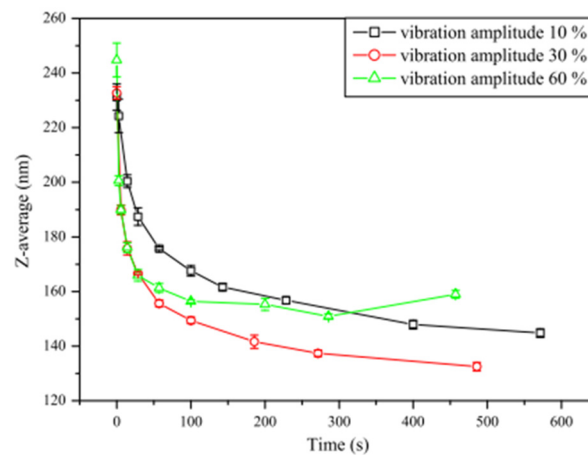


Figure 18. Effect of sonication time (pulse ratio 0.1/2.0 (s/s)) on average cluster size of alumina NF at different vibration amplitudes. Adapted from [179].

3.1.7. Thermal Performance of Heat Transfer Devices

The impact of surfactant (Triton X-100) weight concentration (0.1–0.3 wt%) and NF (TiO_2/DW) weight concentration (0.3–1.2 wt%) on the overall heat transfer coefficient, thermal resistance, and thermal efficiency of the thermosyphon heat pipe (THP) under varying input powers (100–200 W) and inclination angles (45–90°) were investigated [181]. The results reveal an enhancement in the thermal efficiency of THP with an increase in input power, whereas the reverse is observed for the thermal resistance. Maximum thermal efficiency (94%) and overall heat transfer coefficient (285 $\text{W}/\text{m}^2 \text{K}$), and minimum thermal resistance (0.186) of THP are reached using 200 W of input power and 90° inclination angle, and at optimal 0.2 wt% Triton X-100 and 1 wt% TiO_2 NF. Relatively low wall temperature is also achieved using these optimal values at 200 W and 90° inclination. The use of the surfactant reduces the surface tension and increases the stability of the MNF, leading to an enhancement in the heat transfer rate (evaporator), overall heat transfer coefficient, and thermal efficiency of the THP. These findings stress the need to obtain an optimum NF and surfactant concentration in NF studies to achieve better and more reliable results.

The influence of sonication time (1–4 h) on the κ , μ , outlet temperature, electrical, and thermal efficiency of CuO/DW NFs (0.05–0.2 vol%) as coolants in a photovoltaic–thermal solar collector is studied [182]. The results reveal that an increase in the sonication time causes an increase in κ (3.5%), outlet temperature (>65 °C), thermal and electrical efficiency, and a decrease in μ , all as functions of volume concentration. At sonication time of 4 h and volume concentration of 0.2 vol%, optimum κ , μ (7.5%), outlet temperature (>65 °C), power (24.8 W), electrical (15.1%), and thermal efficiency (80.7%) are achieved. It is worth

stating that the optimum outlet temperature, power, electrical, and thermal efficiency are achieved at noon and a photovoltaic panel temperature of 45 °C. However, no scientific stability test is carried out except for the visual inspection. This work emphasized the need to optimize sonication variables to enhance the stability, thermophysical properties, and heat transfer performance of NFs thermal transporting systems.

The influence of sonication time (20–40 min) corresponding to the sonication energy density of 57 J/g–290 J/g on the stability, κ , μ , h , and Nu of 1 wt% MWCNT/DIW + 0.25 wt% GA NF employed as a thermal fluid in a horizontal tube under laminar flow ($Re = 600$ – 1200) was studied [155]. Increasing the sonication time from 20 min to 40 min results in the enhancement of κ , μ , h , and Nu , which reduces as the sonication time is increased from 40 min to 80 min. Thus, the most stable MNF is achieved at a sonication time of 40 min. Sonicating the MNF for 40 min is shown to yield the highest enhancement of κ (20%), μ , h (32% at $Re = 600$), and Nu . In addition, the optimum sonication time (40 min) leads to the highest flow consistency index and lowest flow behavior index, as the MNF demonstrates a non-Newtonian behavior. Figure 19 shows the influence of sonication time on the convective heat transfer coefficient of MNF.

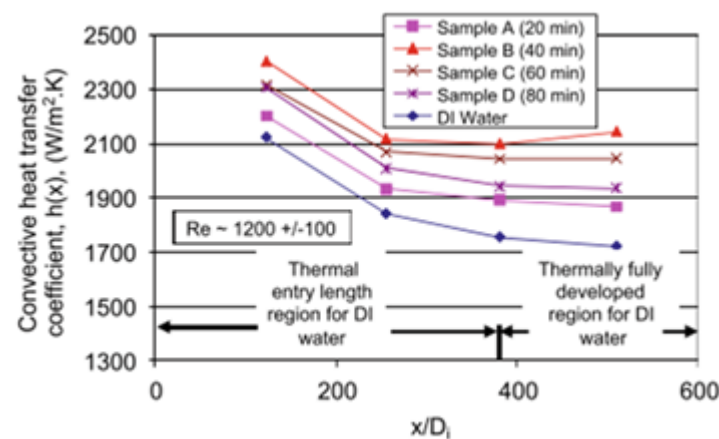


Figure 19. Axial variation of heat transfer coefficient at $Re = 1200 \pm 100$ under varying sonication time using MNF. Adapted from [155].

The effect of sonication power (30%, 60%, and 90% of power), nano-size (20, 40, and 60 nm), and surfactant (SDS) weight concentration (0.05, 0.07, and 0.09 wt%) on the stability and pool boiling heat transfer performance of CuO/DIW NFs (0.025–0.125 wt%) was studied [67]. The results prove that an optimal sonication power of 60%, nano-size of 20 nm, and 0.05 wt% SDS engaged in the formulation of 0.125 wt% CuO/DIW NF yields the highest boiling heat transfer coefficient enhancement of 38.93%. The weight concentration of CuO NF, mass fraction of SDS, nano-size, and sonication power are observed to influence the heat transfer performance of MNF in boil pooling studies. The sonication power is noticed to contribute the most to the boiling heat transfer coefficient.

A study of the influence of nano-size (8 and 20 nm), weight concentration (0.01–0.2 g/L), and sonication time (30 and 120 min) on the AC breakdown voltages of CNT-transformer oil NF was performed [89]. The higher sonication time (120 min) is observed to produce higher breakdown values for all the studied concentrations compared to 30 min of sonication. This is attributed to the dissipation of more energy at 120 min of sonication, which enables the homogenization and stability of the studied NF. The influence of sonication duration (1–3 h) and moisture (0–210 ppm) on the stability, breakdown voltage, and heat transfer performance of transformer oil-based Al_2O_3 (0–0.16 vol%) NFs was examined [183]. An increase in the moisture content is observed to reduce the breakdown voltage. At a sonication time of 3 h and using the 0.1 vol% sample, the highest breakdown voltage and heat transfer performance are recorded. Table 5 presents the preparation, stability, properties, and performance characteristics of some mono NFs.

Table 5. Preparation characteristics, stability tests, properties, and performance of mono NFs.

Reference	NFs	Vol%	Nano-Size	Surfactants	Sonication Time	Stirring Time	Measured Parameters	Stability Test
Kamalgharibi et al. [86]	CuO/EG, DIW, EG-DIW (50:50 vol%)	0.1–0.4 wt%	40–50	PVP, SDS, and Triton X100 (@ 1% vol. of NF) (2-step)	60–270 min at 18–24 KHz	60–75 min	Sedimentation height (75 days)	Sedimentation method/visual inspection
Li et al. [164]	Cu/EG	1–3.8 wt%	50 nm	No surfactant (2-step)	15–75 min @ 20–50 °C	20 min	μ (30 days)	Visual
Abadeh et al. [87]	Fe ₃ O ₄ /DW	1% (wt)	20–30 nm	Citric acid, CTAB, SDS, GA, and Tween 80 (2-step)	20–60 min (initial); 0–40 min @ 100 amplitude	30–90 min @ 50 °C and 400–800 rpm	pH	ZP
Afzal et al. [147]	ZnO and CuO/DIW	0.1 wt%	CuO—30–50 nm ZnO—90 nm	OA and EBT (0.1 wt%) (2-step)	2–8 h	35 min	pH, μ , κ , c_p , specific gravity (24 days)	UV, ZP, visual inspection
Mahbubul et al. [123]	Al ₂ O ₃ /W	0.5 vol%	13 nm	No surfactant (2-step)	1–5 h @ amplitude 50%, pulse on 2 s and pulse off 2 s	-	μ , κ , and volume concentration	ρ and sedimentation
Mahbubul et al. [124]	TiO ₂ /DW	0.5 vol%	21 nm	No surfactant (2-step)	30–180 min @ amplitude 50%, pulse on 2 s and pulse off 2 s	-	Cluster size, ZP, pH	ZP
Asadi et al. [151]	Mg (OH) ₂	0.1–2 vol%	20 nm	CTAB, oleic acid, and SDS (2-step)	10–160 min	-	κ	ZP, visual
Wang et al. [106]	Cu and Al ₂ O ₃ /W	0.05–0.8 wt%	Al ₂ O ₃ -25 nm	SDBS (0–0.15 wt%) (2-step)	15 min	-	pH, particle size, ZP, and κ	ZP
Wang and Li [129]	Cu and Al ₂ O ₃ /W	0.01–0.4 wt%	Al ₂ O ₃ -15–50 nm Cu—25–60 nm	SDBS (2-step)	-	-	pH, μ , and κ	-
Wang and Li [177]	Cu and Al ₂ O ₃ /W	0.01–0.4 wt%	Al ₂ O ₃ -15–50 nm Cu—25–60 nm	SDBS (0–0.14 wt%) (2-step)	1 h	-	pH, and κ	ZP, UV,
Seong et al. [152]	GNP/DW	0.1 wt%	4 nm	SDBS and SDS (1:3–3:1) of GNP	40 min	-	ZP, κ	ZP, visual, and UV
Khooshechin et al. [67]	CuO/DIW	0.025–0.125wt%	20, 40, and 60 nm	SDS (0.05–0.09 wt%)	30%–90% of power	-	κ , h, HTC,	-
Wei et al. [153]	WO ₃ /EG	0.005–5 wt%	40 nm	-	15–60 min	Not mentioned	κ	ZP
Cacua et al. [126]	Al ₂ O ₃ /DIW	0.1 wt%	<50 nm	CTAB (0.036 g) and SDBS (0.064 g) (2-step)	20 min @ amplitude of 30%	-	pH, ZP, PI, average particle size	Visual, ZP, and UV
Asadi and Alarifi [149]	MWCNT/W	0.1–0.5 vol%	-	No surfactant (2-step)	10–80 min	2 h	ZP, μ	ZP, visual
Asadi et al. [148]	MWCNT/W	0.1–0.5 vol%	<7 nm	No surfactant (2-step)	10–80 min	2 h	ZP, κ	ZP, visual
Michael et al. [83]	Al ₂ O ₃ /DW	0.5–2 vol%	13 nm	PVP (2-step)	30–150 min	1 h	κ and μ	ZP (particle size)
Ghorabee et al. [181]	TiO ₂ /DW	0.3–1.2 wt%	20 nm	Triton X-100 (0.1–0.3 wt%)	5 h @ 50 °C	-	Wall temperature, thermal resistance and efficiency and h	-
Adio et al. [74]	Al ₂ O ₃ /GL	1–5 vol%	20–30, 80, and 100 nm	No surfactant (2-step)	1–8 h @ amplitude = 75%, 8 s—on and 2 s—off	Energy density (5 × 10 ⁶ –4 × 10 ⁷ kJ/m ³)	μ , energy density, average particle size	UV, ZP, visual
Adio et al. [98]	MgO/EG	1–5 vol%	21, 105, and 125 nm	No surfactant (2-step)	30–180 min	Energy density (2.18 × 10 ⁶ –13.9 × 10 ⁶ kJ/m ³)	μ , energy density, pH, average particle size	UV, ZP, visual

Table 5. Cont.

Reference	NFs	Vol%	Nano-Size	Surfactants	Sonication Time	Stirring Time	Measured Parameters	Stability Test
Adio et al. [120]	MgO/EG	1–3 vol%	20 and 100 nm	No surfactant (2-step)	30–180 min	Energy density (2.18×10^6 – 13.9×10^6 kJ/m ³)	σ , energy density, pH	ZP, visual
Amrollahi et al. [166]	MWCNT/EG	0.5–2.5 vol%	1–4 nm	No surfactant (2-step)	1–24 h	-	κ	Sedimentation
Graves et al. [174]	Cu/methanol	0.1% wt/vol	25–75 nm	(Cap agent 3-Aminopropyl) trimethoxysilane (175 μ L) (no surfactant; 2-step)	30 min @ amplitude (20–100%)	-	κ , particle size and cluster, ZP, PI	ZP, UV, visual
Mahbubul et al. [150]	Al ₂ O ₃ /DW	0.5 vol%	13 nm	No surfactant (2-step)	0.5–5 h @ amplitude of 50%, 2 s—on and 2 s—off.	Agitated for 1 min	κ , ρ , cluster size, and μ	ZP,
Rajendiran et al. [182]	CuO/DW	0.05–0.2 vol%	27 nm	No surfactant (2-step)	1–4 h	Stirrer	κ , μ , thermal and electrical efficiency	Visual inspection
Nasiri et al. [156]	SWCNT, FWCNT, DWCNT, MWCNT	0.25 wt%	SWCNT-1-1 nm, FWCNT-5 nm, DWCNT-2–4 nm, MWCNT <10 nm and 10–20 nm	1-step and 2-step (no surfactant)	Functionalized, bath (45 min), and probe (45 min with 25% amplitude)	-	κ	-
Ghadimi and Metselaar [157]	TiO ₂ /DW	0.1 wt%	25 nm	SDS (2-step)	Bath (3 h), probe (15 min)	-	κ and μ	UV, Visual, ZP, nanosize
Xia et al. [158]	α Al ₂ O ₃ /DIW	0.1–2.5 vol%	13 nm	SDS and PVP (2-step) @ 0.25–4 wt%	0.25–2 h	-	κ and particle size	Visual
Mahbubul et al. [167]	Al ₂ O ₃ /DW	0.5 vol%	13 nm	No surfactant (2-step)	0.5–5 h @ amplitude of 50%, 2 s—on and 2 s—off.	Agitated for 1 min	cluster size and μ (under shear rate (36.7–305.8 s ⁻¹))	-
Mahbubul et al. [168]	Al ₂ O ₃ /DW	0.5 vol%	13 nm	No surfactant (2-step)	1–5 h @ amplitude of 50%, 2 s—on and 2 s—off.	Agitated for 1 min	Yield stress (under shear rate (12.23–305.8 s ⁻¹))	-
Mahbubul et al. [165]	Al ₂ O ₃ /DW	0.5 vol%	13 nm	No surfactant (2-step)	0–180 min @ amplitude of 50%, 2 s—on and 2 s—off.	Agitated for 1 min	cluster size, particle size, ZP, and μ	ZP, sedimentation
Sadeghi et al. [159]	γ Al ₂ O ₃ /DIW	1–3 vol%	25 nm	(2-step)	15–180 min	-	PI, ZP, UV, average cluster size, and κ	ZP, UV,
Nguyen et al. [179]	Al ₂ O ₃ /W	1 mg/ml	13 nm	PVA (2-step)	30–180 s @ amplitude (10%, 30%, and 60%), pulsed (0.1/0.1 and 1.0 and 1.0), and continuous (30 s and 90 s).	-	ZP and cluster size	ZP and visual inspection
Yang et al. [160]	MWCNT	0.21 vol%	-	Polysisobutene succinimide (0.3–8 wt%)	5–30 min @ energy density (2.4×10^5 – 1.45×10^6 kJ/m ³)	-	κ , μ , stress, aspect ratio	-

Table 5. Cont.

Reference	NFs	Vol%	Nano-Size	Surfactants	Sonication Time	Stirring Time	Measured Parameters	Stability Test
Kole and Dey [161]	ZnO/EG	0.5–3.75 vol%	30–40 nm	No surfactant (2-step)	4–100 h	-	κ and cluster size	Sedimentation
Yu et al. [162]	MWCNT/DW	0.1–1.4 wt%	10–20 nm	SDS @ 0.01–0.4 wt% (2-step)	5–120 min	-	Absorbance	UV
Garg et al. [155]	MWCNT/DIW	0.1 wt%	10–20 nm	GA @ 0.25 wt% (2-step)	20–80 min @ 57 J/g—290 J/g	5 min	κ , μ , h, and Nu	Visual
Lee et al. [173]	γ -Al ₂ O ₃ /DIW	0.01–0.3 vol%	30 ± 5 nm	No surfactant (2-step)	5–30 h	-	ZP	ZP, Visual
Ruan and Jacobi [163]	MWCNT/EG	0.5 wt%	10–20 nm	GA @ 0.25 wt% (2-step)	5–1355 min @ continuous and pulse (0.8 s—on and 3.2 s—off)	-	κ , μ , γ , average cluster size, CNT length	visual
Yu et al. [175]	SWCNT/DIW	0.025 w/v%	-	1 w/v% sodium deoxycholate	10–120 min (3 mm and 6 mm tip) @ 20–120 W	-	Absorbance	UV
Elcioglu and Murshed [176]	ZnO/DW	0.05–0.4 vol%	15–20 nm	No surfactant (2-step)	0.5–4 min @ amplitude 40% and 100%	30 min	Surface tension	-

3.2. Hybrid NFs

3.2.1. Thermal, Optical, and Rheological Properties

The influence of stability via the functionalization (solvothermal technique) of MWCNT- γ -Al₂O₃/DIW (volume fraction of 0.2–1) NFs on κ was examined [72]. The ZP is used to check the stability of the HNFs. The κ of the functionalized HNF is the highest, with an enhancement of 20.68% over the base fluid. Moreover, the highest stability is recorded for the functionalized HNF with a ZP of -22.3 mV. This emphasizes the impact of functionalization on stability and κ . The effect of the sonication time (0.5–4 h) on κ of DW-based Ag- γ -Al₂O₃ NFs (0.005–0.1 vol%) was investigated [79]. The PVP is used as a surfactant for formulating the HNF, while the mixing ratios of 30:70, 50:50, and 70:30 are employed in the study. The HNF with a mixing ratio of 50:50 is noticed to have the highest κ compared to others. The optimum κ of Ag- γ -Al₂O₃ (50:50)/DW NF is achieved at a sonication time of 2 h, after which reduction is noticed.

The stability of DW-based ternary NFs (CuO-MgO-TiO₂) with a concentration of 0.1–0.5 vol% via the mixing ratios (33.4:33.3:33.3, 50:25:25, 60:30:10, 25:50:25, and 25:25:50), sonication time (20–150 min), and the mass percent of SDS was optimized [78]. The stability is examined using stability time and ZP. The most stable is the HNF, with a mixing ratio of 60:30:10 achieved using a sonication time of 120 min, 0.49 mass% of SDS, a stability time of >40 h, and a ZP of >35 mV. They showed that increasing the sonication power and time enhanced the κ of HNF with a mixing ratio of 60:30:10 to a certain point before it is reduced. The maximum κ is achieved at optimum values of 420 W (sonication power) and 140 min (sonication time). The stability is observed to slightly reduce as the concentration of the HNF increases. The stability of MgO-TiO₂/DW NF with volume concentrations of 0.1–0.5 vol% under varying sonication times (20–80 min), mixing ratios (50:50, 80:20, 20:80, 60:40, and 40:60), and SDS weight concentrations, was investigated [84]. The HNF with a mixing ratio of 50:50 has the best stability, as indicated by the highest values of ZP (>38 mV) and stability time (>80 h) and achieved by sonicating for 60 min and using 0.35 wt% of SDS. The highest value of κ is obtained for the HNF with an 80:20 mixing ratio, which is attained at an optimum sonication time of 75 min and sonication power of 350 W.

The effect of stability of DIW-based Cu-Al₂O₃ NFs (0.0005–0.0105%) at different mixing ratios (0.3:0.7, 0.5:0.5, and 0.7:0.3) on the κ , ρ , and μ via the effective particle diameter, sedimentation velocity, PI, and ZP was investigated [184]. Results show that after 240 h, the HNF with a 0.5:0.5 mixing ratio has the best stability as recorded by the high ZP (>40 mV) moderate polydispersity index, and low sedimentation velocity and particle diameter. The stability of the HNFs over 240 h reveals a slight decrease in κ , ρ , and μ until 50 h; thereafter, constant values are observed. The most stable HNF (Cu-Al₂O₃ (0.5:0.5)) exhibits the highest κ and ρ , and the lowest μ .

The effect of sonication time (30–120 min), dispersion fraction of SDS (0.6–1.2%), and sonication amplitude (70–80%) on the stability, pH, and σ of DIW-based MgO, ZnO, and MgO-ZnO NFs (0.1 vol%) was optimized [77]. The visual inspection and absorbency tests are used to determine the stability of the MNFs and HNFs. An optimum sonication time of 45 min, dispersion fraction of 1%, and amplitude of 75% are reported to achieve optimum stability via the measurement of pH and σ (see Figures 20 and 21). The stable condition is reached by obtaining the CMC at the point of inflection of pH and σ for the investigated parameters of the sonication time and amplitude, and dispersion fraction. In addition, optimum stability and pH of fMWCNT- γ -Fe₂O₃ (20:80) NFs (0.1–1.5 vol%) are achieved with an optimal sonication time of 2 h, dispersion fraction (SDS) of 0.5%, and amplitude of 70% [4] (see Figure 21). The σ is measured to determine the CMC of the HNF for each optimized parameter to achieve stable HNFs via the visual inspection and absorbency test. A similar result is obtained by [66] for the formulation of fMWCNT- γ -Fe₂O₃ (20:80) NFs (0.1–0.4 vol%).

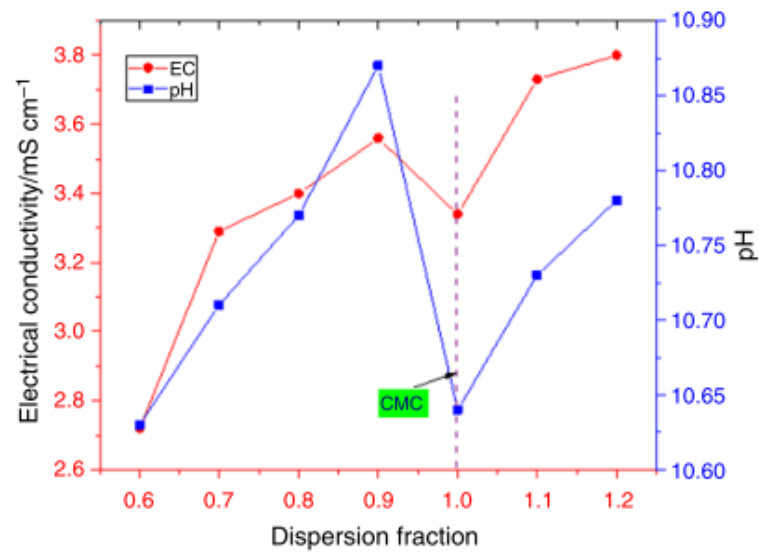


Figure 20. Effect of dispersion fraction on electrical conductivity and pH of 0.5 vol% MgO-ZnO/DIW NF. Adapted from [77].

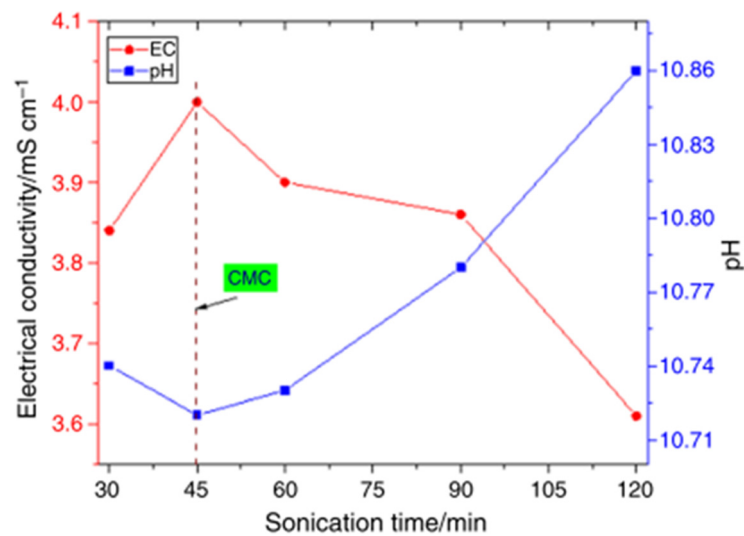


Figure 21. Effect of sonication time on electrical conductivity and pH of 0.5 vol% MgO-ZnO/DIW NF. Adapted from [77].

The stability of EG-DW (40:60 wt%)-based GNP-TiO₂ and GNP NFs (0.025–0.1 wt%) using different surfactants (PVP, SDS, SDC, CTAB, Triton X100, and SDBS at 1:1), sonication time of 15–90 min, sonication amplitude of 60%, stirring rate of 500 rpm, and stirring time of 30 min for HNFs and 10 min for MNFs was investigated [81]. The stability is monitored using the absorbency test, sedimentation technique, and ZP. The MNFs are observed to be slightly more stable than the HNFs for all cases studied. The most stable HNF and MNF used CTAB as a surfactant and was sonicated for 90 min.

The influence of sonication time (60–240 min), dispersion fractions (0.8–1.3%) of SDS and SDBS, sonication amplitude (50–70%), and frequency (60–80%) on the stability of DIW- and DIW-EG (50:50)-based γ -Al₂O₃- γ -Fe₂O₃ (25:75) NF (0.1 vol%) as measured using σ was investigated [75]. Optimum stability, as related to the CMC, is reached at an optimal sonication time, amplitude, and frequency of 120 min, 70%, and 70% and using 1.1% SDS and 1.12% SDBS for DIW- and EG-DIW based HNF, respectively. The optimal values are obtained at CMC, which is achieved when there is the inflection of σ values (maximum or minimum).

The effect of different surfactants (7), temperature (55–80 °C), base fluids (4), and sonication duration (30–240 min) on the viscosity and stability of MWCNT (20%)-CeO₂ (80%) NFs was investigated [91]. The most stable HNF, as revealed by the ZP measurement, is the Benzalkonium chloride-based MWCNT-CeO₂ NF, while the Span-80-based HNF is the worst. The optimum sonication time corresponding to the peak stability of the HNF is found to depend on the base fluid type in the formulation of the HNFs (therminol VP-I—60 min, DIW—60 min, EG—90 min, and silicone oil—120 min). Viscosity is observed to reduce up to the optimum sonication time and then increases with DIW-based HNF found to demonstrate the lowest marginal viscosity and long-term stability.

The stability, κ , and σ of DIW-based CeO₂-MWCNT NFs under varying sonication time (30–180 min), pH (8–11), surfactants (six), and surfactant fractions (5:0, 4:1, 3:2, 2:3, and 1:4), and preparation days (15–90 days) were studied [88]. The test samples are formulated using $\phi = 0.25$ –1.50 vol% and subjected to temperature variation of 25–50 °C. The optimum sonication time of 90 min, pH of 9.5, and surfactant fraction of 3:2 is observed for all the tested samples with 30 days and 90 days of optimum stability using CTAB and SDBS, respectively. At the optimum conditions and using CTAB, κ is improved by 27.38% using the 1.50 vol% sample and at 50 °C, while σ is enhanced by 30.1% using SDBS (4:1).

3.2.2. Zeta Potential and Absorbance

The effect of pH on the stability, μ , κ , and σ of naphthenic oil-based SiO₂ and SiO₂-GNP NFs (0.01–0.08 wt%) was explored [132]. The stability of both MNFs and HNFs is checked using ZP, absorbency test, sedimentation rate, and visual inspection. The NFs are formulated at four different pH values (9, 10, 11, 12), with those at pH 11 found to be the most stable, as indicated by all the stability tests conducted. The instability of NF samples with pH 9, 10, and 12 is observed to reduce the μ , σ , and ZP and increase the κ . It is noted that the addition of SiO₂ NPs to GNP NPs improved the stability, μ , and κ of HNFs, and it also reduced σ .

The stability of Al₂O₃ + TiO₂ + SiO₂/EG-W (40:60 vol%) NFs at concentrations of 0.05–0.3 vol% using sedimentation, absorbency, ZP, and visualization techniques was studied [109]. Test samples are sonicated for 0.5–10 h. The individual MNF is mixed at a ratio of 0.33 to formulate the HNF. The results reveal that as the sonication time increases, the concentration ratio of the HNF increases. At an optimum sonication time of 10 h, the HNF is stable with a ZP of 25.1 mV. After 14 days, the sample remains stable, with an 80% concentration ratio and its absorbance also remain constant for 10 days.

3.2.3. Photothermal Conversion and Solar Collector Performance

The impact of pH, sonication time (20–120 min), and mass fraction of Sodium hexa meta phosphate (SHMP) as a surfactant on the stability of EG- and EG-W (50:50)-based γ -Al₂O₃, CuO, and γ -Al₂O₃ + CuO NFs for direct absorption solar collectors was investigated [134]. Generally, absorbance is observed to increase with pH rise and thereafter decrease as pH increases. The reverse is noticed for non-dimensional μ with pH. The results showed that for the EG-based NFs, the optimal pH, sonication time, and SHMP mass fraction are 8.5–10, 6.5–7.5, and 7–8.2, 120 min, 55 min, and 100–120 min, and 1.65, 0.5, and 1.5 for CuO, γ -Al₂O₃, and γ -Al₂O₃ + CuO, respectively. For the EG-W (50:50)-based NFs, the optimal pH, sonication time, and SHMP mass fraction are 8–9, 7–8, and 7.2–8.5, 120 min, 40–50 min, and 100–120 min, and 1.75, 0.25–0.5, and 1.35 for CuO, γ -Al₂O₃, and γ -Al₂O₃ + CuO, respectively. At optimal stability conditions, the peak absorbance is found to correspond to the lowest non-dimensional μ . Owing to the stability of the NFs, the extinction coefficient and absorbance of the HNFs are observed to be around the same value as the addition of the extinction coefficient of individual MNFs. The extinction coefficient of EG-W-based NFs is observed to be higher than that of those EG-based NFs.

A similar study to [134], in which only the base fluid is changed to DW from EG-W and EG [85], reported the optimal SHMP mass concentration, pH, and sonication time of 1.5, 0.25–0.5, and 1.25, 8–9, 7–8.2, and 7.5–8.5, and 100–120, 45, and 100–120 min for

DW-based CuO, $\gamma\text{Al}_2\text{O}_3$, and $\gamma\text{Al}_2\text{O}_3 + \text{CuO}$ NFs, respectively. These reported optimal values corresponding to the minimum viscosity of the MNFs and HNFs are achieved at optimal stability conditions leading to optimal absorbency and extinction coefficient. The influence of sonication time (30–240 min) on the stability, pH, and evaporation rate of MWCNT-GNP/seawater NFs (0.001–0.04 wt%) was investigated [71]. The ZP, visual inspection, and absorbency tests are used to check the stability of the HNFs. Increasing the sonication time is observed to increase the ZP and pH values, which decreased as sonication time is further increased. An optimal sonication time of 120 min is observed at which maximum values of pH (7–8), ZP (40.6 mV), absorbency, temperature rise (26.9 °C), light intensity, and evaporation efficiency (61.3%) are recorded, along with the minimum values of evaporation rate and average particle size. An increase in the volume concentration of the HNF results in the ZP reduction. At 0.01 wt%, sonication time of 120 min, and 3.6 suns, maximum evaporation efficiency and minimum evaporation rate are achieved.

The response surface methodology was employed to optimize the mass fraction of ATO-Ag/DIW NFs (0.01–0.2 wt%) and SDS as a surfactant (0.1–0.2 wt%) to maximize κ and solar-weighted absorption percentage [125]. The visual inspection and UV methods are used to monitor the stability of the HNFs. With 0.2 wt% ATO-Ag/DIW NF + 0.15 wt% SDS, a maximum κ of 0.67 W/mK and solar-weighted absorption percentage of 98.90% are obtained. The optimal value of 0.1 wt% for both the HNF and surfactant is achieved using the response surface methodology leading to a solar-weighted absorption percentage of 90.12%. The optimized 0.1 wt% HNF + 0.1 wt% SDS is observed to be more stable than 0.2 wt% HNF + 0.15 wt% SDS, especially for a long time (150 days). The optimized 0.1 wt% HNF + 0.1 wt% SDS is subsequently studied for its thermal performance as a thermal fluid in a direct absorption solar collector. A correlation was proposed to estimate the solar-weighted absorption percentage of the optimized HNF based on the mass fraction of the HNF and surfactant.

Similarly, a response surface methodology scheme was used to optimize the mass fractions of CuO (100–1500 mg/L) + SiO₂-Ag (100–1500 mg/L) NFs and SDS mass fraction (200–2000 mg/L) to achieve a stable HNF with maximum κ and solar-weighted absorption fraction [64]. The UV technique is used to measure stability. Results demonstrate that the highest solar-weighted absorption fraction (82.84%) is achieved with CuO, SiO₂/Ag, and SDS of 383.3, 383.3, and 1614.9 mg/L, respectively. Moreover, with mass fractions of 1216.2, 383.3, and 1614.9 mg/L for CuO, SiO₂/Ag, and SDS, respectively, the maximum κ ratio (1.234) is reached. By optimizing via response surface methodology, the optimal mass fractions are 864.7 mg/L (CuO), 206.3 mg/L (SiO₂/Ag), and 1996.2 mg/L (SDS) leading to relative κ of 1.231, solar-weighted absorption fraction of 81.78%, and ZP of 38.7 mV. The most significant variable that contributed to the estimation of the relative κ and solar-weighted absorption fraction is the SDS mass fraction. This is found to be contrary to the work of [125], which reported the ATO-Ag (HNP) as the most significant variable in estimating the same. Similar to the work of [125], mathematical regressions are developed to predict the relative κ and solar-weighted absorption fraction of the HNF subject to the mass fractions of CuO, SiO₂/Ag, and SDS.

The influence of pH (2–10), surfactant (SHMP) mass fraction (0.2–2%), and sonication time (20–120 min) on the stability, absorption, and κ of DW- and EG-DW (50:50)-based CuO (0.001 vol%)- $\gamma\text{Al}_2\text{O}_3$ (0.04 vol%) NF was studied [135]. A stability check is carried out using UV and visual tests. The optimal pH, surfactant mass fraction, and sonication time of 7–8.2 and 7.5–8.5, 1.35 and 1.25, and 100–120 min for EG-DW- and W-based CuO- $\gamma\text{Al}_2\text{O}_3$ NF, respectively, are reported. It can be noticed that, at optimal stability conditions, maximum absorbance, and κ are recorded. Thus, revealing the dependence of the stability and κ of CuO- $\gamma\text{Al}_2\text{O}_3$ NF on sonication time, surfactant mass fraction, and pH. The optimized HNF is further studied as a thermal fluid in a direct absorption solar parabolic trough collector.

3.2.4. Thermal and Hydraulic Performance of Heat Transfer Devices

The influence of surfactants (SDS and PVP) on the thermal performance (Nu , ΔP , and η) of DW-based Al_2O_3 -Ag NF (0.2 vol%) used as a thermal fluid in a helical heat exchanger was investigated [65]. The weight concentrations of each surfactant are between 0.1 and 0.4 wt%. The results prove that the use of SDS at an optimum concentration of 0.1 wt% leads to the highest heat transfer performance enhancement of 16% compared with DW. At a Reynolds number of 5100, 0.1 wt% SDS + HNF yields a maximum Nu enhancement ratio of 6.28, a minimum ΔP enhancement ratio of 1.03, and a maximum thermal performance ratio of 1.16. Figures 22 and 23 show the effect of different surfactant types and concentrations on the heat transfer enhancement ratio and thermal efficiency of HNFs in a helical heat exchanger, respectively. To investigate the heat transfer performance of $TiO_2 + SiO_2$ (50:50)/W-EG (60:40 vol) NFs (0.5–0.3 vol%) in a tube under turbulent flow, [82] optimized the sonication time (0–2 h) for better stability and performance of the HNFs. Visual inspection and absorbency tests are used to monitor stability. After 270 h of storage, the ratio of absorbance showed that the optimal sonication time of 1.5 h yielded the most stable HNF. Table 6 presents the preparation, stability, properties, and performance characteristics of some HNFs.

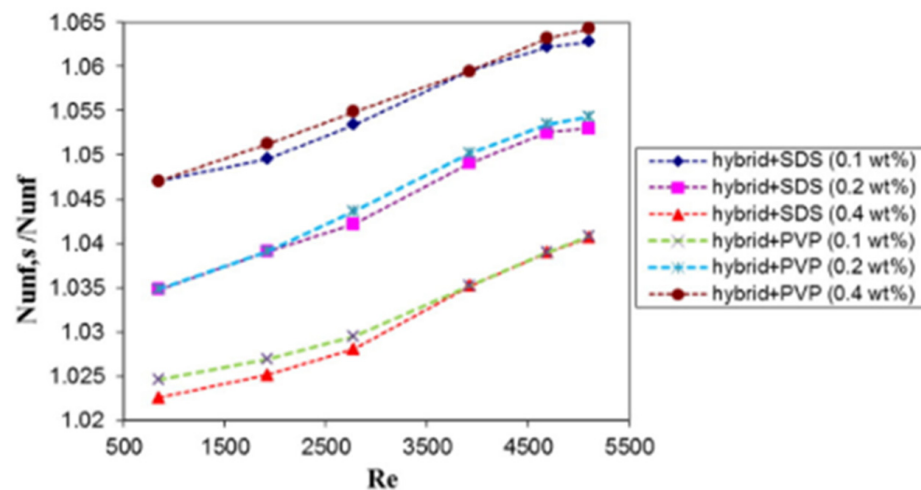


Figure 22. Nusselt number enhancement ratio against Reynolds number for hybrid NF at different concentrations of surfactant (SDS or PVP). Adapted from [65].

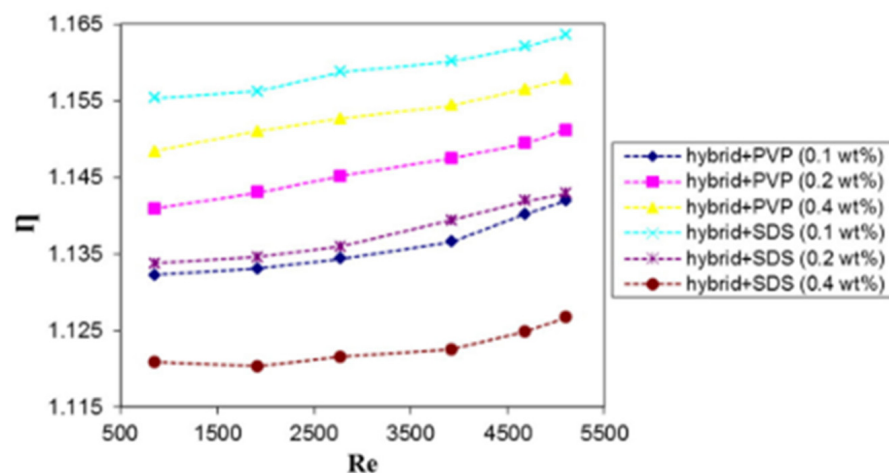


Figure 23. Thermal efficiency against Reynolds number for helical coil with hybrid NF containing SDS or PVP Adapted from [65].

Table 6. Preparation characteristics, stability tests, properties, and performance of hybrid NFs.

Reference	NFs	Vol%	Nano-Size	Surfactants	Sonication Time	Stirring	Measured Parameters	Stability Test
Xian et al. [81]	GNP-TiO ₂ (50:50 wt%)/DW-EG (60:40 wt%)	0.025–0.1 wt%	GNP—5 nm TiO ₂ —<4 nm	CTAB, PVP, Triton X100, SDS, SDC, SDBS, (1:1 conc. of NP) (2-step)	15–90 min @ 60% amplitude	30 min and 500 rpm	Absorbance and ZP (40 days)	Sedimentation method, UV, and ZP
Abbasi et al. [72]	f-MWCNT- γ -Al ₂ O ₃ (1:1 wt%)/DIW	0.1 wt%	f-MWCNT—OD = 10–50	GA (0.01 VF) (2-step)	1 h	-	κ (45 days)	Visual
Shahsavari et al. [146]	(CNT + Fe ₃ O ₄)/DIW	CNT—0.11–1.535 wt% Fe ₃ O ₄ —0.494–2.428 wt%	CNT—10–30 nm Fe ₃ O ₄ —13 nm	GA (0.026–0.227)—CNT and TMAH (0.046–0.227)—Fe ₃ O ₄ (2-step)	2.5–10 min	-	κ (30 days)	visual
Aparna et al. [79]	γ -Al ₂ O ₃ -Ag/DW (50:50, 30:70, 70:30)	0.005–0.1 vol%	Ag—3–25 nm γ -Al ₂ O ₃ —5–30 nm	PVP (2-step)	0.5–4 h @ 5 min (on) and 3 min (off)	4 h	κ (24 h)	ZP, visual
Qing et al. [132]	SiO ₂ -GNP/naphthenic oil	0.01–0.08 wt%	-	No surfactant (2-step)	4 h	-	pH, μ , κ , and σ (350 h -sedimentation, 14 days visual inspection)	Sedimentation rate, visual, ZP, UV
Mousavi et al. [78]	CuO-MgO-TiO ₂ /DW (60:30:10)	0.1–0.5 vol%	CuO—40 nm MgO—25–45 nm TiO ₂ —18–23 nm	SDS (2-step)	20–150 min sonication power (350–400 W)	90 min	κ (30 days)	ZP, stability time
Mousavi et al. [84]	MgO-TiO ₂ /DW (50:50)	0.1–0.5 vol%	MgO—25–45 nm TiO ₂ —18–23 nm	SDS—0.35 wt% (2-step)	20–100 min with sonication power (250–370 W)	60 min	κ (>3 days)	ZP, stability time
Siddiqui et al. [184]	Cu-Al ₂ O ₃ /DIW (0.3:0.7, 0.5:0.5, and 0.7:0.3)	0.0005%–0.0105%	Cu—25 nm Al ₂ O ₃ —13 nm	No surfactant (2-step)	10–30 min	No stirring	κ , μ , and ρ (240 h)	Sedimentation velocity, ZP, polydispersity index, and effective diameter
Ramadhan et al. [109]	Al ₂ O ₃ +TiO ₂ +SiO ₂ /EG-W (40:60 vol%) (0.3:0.3:0.3)	0.05–0.3 vol%	Al ₂ O ₃ —13 nm TiO ₂ —50 nm SiO ₂ —30 nm	No surfactant (2-step)	0.5–10 h	120 min	Concentration ratio (14 days)	UV, sedimentation, visual, and ZP
Hormozi et al. [65]	Al ₂ O ₃ -Ag/DW (97.5:2.5)	0.2 vol%	Al ₂ O ₃ —55 nm Ag—25 nm Al ₂ O ₃ -Ag—80 nm	SDS and PVP (0.1–0.4 wt%) (2-step)	-	-	Nu, ΔP , η	-
Menbari et al. [134]	CuO + γ -Al ₂ O ₃ , CuO, and γ -Al ₂ O ₃ /W and EG-W (50:50)	0.0001–0.008 vol%	CuO—40 nm γ -Al ₂ O ₃ — \leq 100 nm	SHMP@ different mass fractions (2-step)	(20–120 min @ amplitude = 70%)	-	pH, μ , absorbance	UV
Menbari et al. [85]	CuO + γ -Al ₂ O ₃ , CuO, and γ -Al ₂ O ₃ /DW	0.0001–0.008 vol%	CuO—40 nm γ -Al ₂ O ₃ — \leq 100 nm	SHMP@ different mass fractions (2-step)	(20–120 min @ amplitude = 70%)	-	pH, μ , absorbance (1 month) pH, temperature rise, particle size, light intensity, evaporation rate, and evaporation efficiency	UV
Ghafurian et al. [71]	MWCNT-GNP/sea water (1:1)	0.001–0.04 wt%	MWCNT- 20–30 nm GNP—40 nm	GA (2-step)	30–240 min	-		UV, ZP, visual

Table 6. Cont.

Reference	NFs	Vol%	Nano-Size	Surfactants	Sonication Time	Stirring	Measured Parameters	Stability Test
Nabil et al. [82]	TiO ₂ + SiO ₂ /W-EG (60:40 vol) (50:50 vol%)	0.5–3 vol%	TiO ₂ —50 nm SiO ₂ —22 nm	No surfactant (2-step)	0–2 h	Not stated	Absorbance (30 days)	UV, sedimentation,
Sreekumar et al. [125]	ATO-Ag/DIW	0.01–0.2 vol%	ATO-Ag—20–50 nm Ag—10 nm	SDS (0.1–0.2 vol%)	-	-	Solar weighted absorption percentage, κ Solar weighted absorption percentage, κ	Visual, UV
Joseph et al. [64]	SiO ₂ /Ag-CuO/DIW		CuO—< 50 nm	SDS (200–2000 mg/L)	15 min	30 min	pH, μ , absorbance (1 month)	UV
Menbari et al. [135]	CuO + γ Al ₂ O ₃ , CuO, and γ Al ₂ O ₃ /EG-DW (50:50)	CuO-0.001 vol% γ Al ₂ O ₃ -0.04 vol%	CuO—40 nm γ Al ₂ O ₃ —100 nm	SHMP (0.2–2%) (2-step)	(20–120 min @ amplitude = 70%	-	κ	-
Asadikia et al. [154]	Fe ₂ O ₃ -MWCNT/EG-W (30–70 v/v)	Fe ₂ O ₃ - 0.1–2% w/v MWCNT- 0.01–1% w/v)	Fe ₂ O ₃ —20 nm MWCNT- 40 nm	-	2 h	-	σ	Absorbance and visual inspection
Giwa et al. 2020a [75]	γ Al ₂ O ₃ - γ Fe ₂ O ₃ /DIW * DIW-EG (50:50) (25:75)	0.05–0.75 vol%	γ Al ₂ O ₃ —20–30 nm γ Fe ₂ O ₃ —20–30 nm	SDS and SDBS (0.8–1.3%) (2-step)	60–240 min @ amplitude (50–70%) and frequency (60–80%)	-	σ and pH	Absorbance and visual inspection
Giwa et al. 2020b [77]	MgO/, ZnO/, MgO-ZnO/DIW (20:80–80:20)	0.1 vol%	MgO—20 and 100 nm ZnO—20 nm	SDS (0.6–1.2%) (2-step)	30–120 min @ amplitude (70–80%)	-	σ	Absorbance and visual inspection
Giwa et al. 2020c [66]	MWCNT-Fe ₂ O ₃ /DIW (20:80)	0.05–0.4 vol%	MWCNT—10–20 nm Fe ₂ O ₃ —20–30 nm	SDS (0.5–1.2%) (2-step)	2 h @ amplitude (70%), 5 s—on and 2 s—off	-	σ	Absorbance and visual inspection
Chakraborty et al. [127]	TiO ₂ and TiO ₂ /Ag	0.1–0.4 wt%	-	No surfactant (2-step)	10–30 min	Stirred	pH	Settling height and time

It is pertinent to mention that the choice of nanoparticles and base fluids to formulate HNFs is critical to their thermal, rheological, and optical properties, photothermal conversion, and convective heat transfer performances and their corresponding applications. The κ , μ , and other thermal properties of nanoparticles and base fluids, the chemical characteristics of base fluids, and the purpose behind the formulation of the HNFs should be carefully considered in choosing the nanoparticles and base fluids to be engaged in various NF-based studies.

4. Future Research Direction

The reviewed literature concerning the influence of the preparation characteristics on the properties and performances of mono and hybrid NFs revealed the huge importance of stability, most especially, the optimum stability conditions to NF research and published results. The complexity of achieving stable conditions for mono and hybrid NFs through the preparation characteristics is also demonstrated. The stability of mono and hybrid NFs is strongly related to the preparation characteristics, such as stirring duration, temperature, and speed, volume, density, and base fluid type, weight/volume concentration, density, nano-size, and type of mono or hybrid NPs used, type and quantity of surfactant used, and finally, the sonication time, mode, temperature, frequency, and amplitude. The future of mono and hybrid NF studies (rheological, optical, and thermal properties and application in diverse areas) is highly dependent on achieving the optimum stability conditions through the optimization of the preparation characteristics, which would yield better, more accurate, and more reliable results, especially in the quest to apply them for improved performance. Stability without stirring and surfactant is observed to be achieved at a relatively longer sonication time. However, this is not the case for most of the cases of MNF and HNF formulation. A schematic diagram of the influence of preparation characteristics on the properties and performance of MNFs and HNFs is provided in Figure 24.

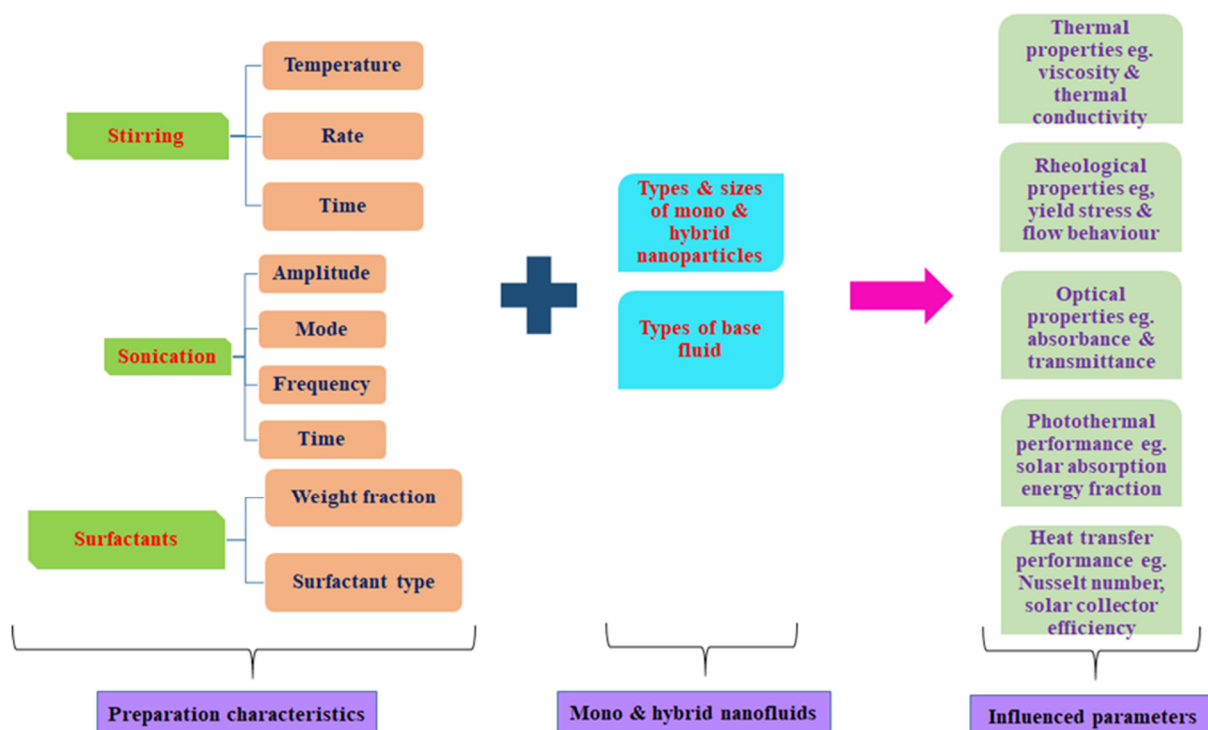


Figure 24. Influence of preparation characteristics on properties (optical, thermal, and rheological) and performance of mono and hybrid NFs.

The stability of mono and hybrid NFs has been researched to affect their pH [85,126,132,135], κ [123,132,152,184], μ [85,123,184], ρ [123,184], σ [132,176], ZP values [78,123,126], aggre-

gate size [164], sedimentation time and velocity [78,184,185], c_p [184], surfactant type and fraction [65,81,185], storage period [123], absorbency, extinction coefficient, and photothermal conversion [64,85,125,135], light intensity and vapor generation [71], coefficient of heat transfer and Nusselt number [65,67,155,181], and pumping power [149]. Except with the same authors or references to formerly published studies, the public domain is inundated with literature on mono and hybrid NF studies in which the results and stability cannot be reproduced. As one of the great attributes of an experiment is the ability to be reproduced, this is largely lacking in mono and hybrid NF studies, which, in our opinion, needs to be addressed urgently in the future.

It can be deduced from the survey of the reviewed literature in this work and publications on NF preparation and stability that there is still no standard procedure for the formulation of NFs based on the two-step strategy, which involved the deployment of sonication. The diverse results published in the open literature through the various ways deployed by different authors to formulate NFs can be strongly linked to the difference in nanoparticles and base fluid types with various chemical compositions and bonding structures, and thus exhibiting diverse stability mechanisms. The use of a suitable and more generalized formulation procedure is envisioned to promote more stable NFs and better results in terms of the differences in NF applications [89].

With the lack of or insufficient preparation characteristics data to reproduce stable mono and hybrid NFs and subsequent results (rheological, optical, and thermal properties and performance), it is essential to provide detailed preparation characteristics data. This will help to reproduce stable NFs and reliable results. With the increasing number of studies on the HNFs and the future investigation of novel base fluids, NPs, HNPs, and areas of application, it is, therefore, necessary for results to conform, which can only be attained through the optimization of preparation characteristics and provision of a detailed report in the literature. In addition, few studies reported the effects of aging and reusability of MNFs and MNFs, tip width of the ultrasonicator probe, sonication temperature, stirring speed and temperature, and mode of ultrasonicators (continuous and pulsed) on the properties and performance of NFs [82,123,163,164,175,179]. Likewise, very limited studies have been carried out concerning the influence of probe-type and bath-type ultrasonicators on the stability and properties of NFs, which is marked by huge discrepancies [156,157]. Furthermore, the functionalization of HNPs and MNPs is observed to produce more stable HNFs and MNFs, of which limited studies have been published in the open literature [72,156]. The published results in this regard require further investigation to substantiate the existing claims.

5. Conclusions

The preparation of mono and hybrid NFs to attain stable conditions is a complex undertaking that involves various parameters, such as stirring duration, temperature, and speed, volume, density, and base fluid type, weight/volume concentration, density, nano-size, and type of mono or hybrid NPs used, type and quantity of surfactant used, sonication time, modes, frequency, and amplitude. From this present work, it is observed that the formulation of diverse mono and hybrid NFs from various types of NPs and HNPs (with different sizes and shapes), and base fluids involved the use of different preparation parameters and the need to optimize these parameters is important to the stability of NFs and their applications in terms of the thermal, optical, rheological, and convective properties, photothermal conversion, and thermal performance. Furthermore, the stability is established to significantly influence the properties and performance of NFs in various applications. As NF preparation is an experimental exercise, the need to reproduce experiments, stability, and results of mono and hybrid NF studies call for the detailed disclosure of the preparation variables deployed in future studies, which could guarantee the convergence of research findings in terms of accuracy, reliability, and improvement.

Author Contributions: Conceptualization, H.Y.; organization and material sourcing, S.O.G. and S.N.; writing—original draft preparation, S.O.G. and S.N.; writing—review and editing, H.Y., S.O.G. and S.N.; supervision, H.Ş.A.; project administration, H.Y. and H.Ş.A.; funding acquisition, H.Y. All authors have read and agreed to the published version of the manuscript.

Funding: This work was supported by the Deanship of Scientific Research, the Vice Presidency for Graduate Studies and Scientific Research, King Faisal University, Saudi Arabia (Grant No. 2276).

Data Availability Statement: Not applicable.

Conflicts of Interest: The authors declare no conflict of interest.

Nomenclature

NP—nanoparticles	h, HTC—coefficient of heat transfer ($W/m^2 K$)
HNF—hybrid nanofluids	W—water
HNP—hybrid nanoparticles	DIW—deionized water
MNF—mono nanofluid	DW—distilled water
TEM—transmission electron microscopy	EG—ethylene glycol
SEM—scanning electron microscopy	C_p —specific heat (J/kgK)
EDL—electrical double layer	ZP—zeta potential
XRD—X-ray diffraction	IEP—isoelectric potential
SHMP—sodium hexa meta phosphate	GL—glycerol
THP—thermosyphon heat pipe	SDS—sodium dodecyl sulphate
UV—ultraviolet	CTAB—cetyl trimethyl ammonium bromide
Nu—Nusselt number	GA—gum Arabic
ΔP —pressure drop	OA—oleic acid
φ —volume concentration	SDBS—sodium dodecyl benzene sulfonate
η —efficiency	TMAH—tetramethylammonium Hydroxide
μ —viscosity (mPas)	CMC—critical micelle concentration
κ —thermal conductivity ($W/m K$)	SDC—sodium deoxycholate
θ —contact angle	PVA—polyvinyl alcohol
σ —electrical conductivity (S/m)	PVP—polyvinyl pyrrolidone
γ —yield stress	EBT—Eriochrome Black T

References

- Sharifpur, M.; Adio, S.A.; Meyer, J.P. Experimental investigation and model development for effective μ of Al_2O_3 -glycerol NFs by using dimensional analysis and GMDH-NN methods. *Int. Commun. Heat Mass Transf.* **2015**, *68*, 208–219. [[CrossRef](#)]
- Rostami, S.; Toghraie, D.; Shabani, B.; Sina, N.; Barnoon, P. Measurement of the κ of MWCNT-CuO/water hybrid NF using artificial neural networks (ANNs). *J. Therm. Anal. Calorim.* **2021**, *143*, 1097–1105. [[CrossRef](#)]
- Osman, S.; Sharifpur, M.; Meyer, J.P. Experimental investigation of convection heat transfer in the transition flow regime of aluminium oxide-water NFs in a rectangular channel. *Int. J. Heat Mass Transf.* **2019**, *133*, 895–902. [[CrossRef](#)]
- Giwa, S.O.; Sharifpur, M.; Ahmadi, M.H.; Sohail Murshed, S.M.; Meyer, J.P. Experimental investigation on stability, μ , and σ of water-based hybrid NF of mwcnt- Fe_2O_3 . *Nanomaterials* **2021**, *11*, 136. [[CrossRef](#)]
- Nwaokocha, C.; Momin, M.; Giwa, S.; Sharifpur, M.; Murshed, S.M.S.; Meyer, J.P. Experimental investigation of thermo-convection behaviour of aqueous binary NFs of MgO-ZnO in a square cavity. *Therm. Sci. Eng. Prog.* **2022**, *28*, 101057. [[CrossRef](#)]
- Rostami, S.; Aghaei, A.; Hassani Joshaghani, A.; Mahdavi Hezaveh, H.; Sharifpur, M.; Meyer, J.P. Thermal-hydraulic efficiency management of spiral heat exchanger filled with Cu-ZnO/water hybrid NF. *J. Therm. Anal. Calorim.* **2021**, *143*, 1569–1582. [[CrossRef](#)]
- Giwa, S.O.; Sharifpur, M.; Meyer, J.P. Effects of uniform magnetic induction on heat transfer performance of aqueous hybrid ferrofluid in a rectangular cavity. *Appl. Therm. Eng.* **2020**, *170*, 115004. [[CrossRef](#)]
- Giwa, S.O.; Sharifpur, M.; Meyer, J.P. Experimental study of thermo-convection performance of hybrid NFs of Al_2O_3 -MWCNT/water in a differentially heated square cavity. *Int. J. Heat Mass Transf.* **2020**, *148*, 119072. [[CrossRef](#)]
- Sharifpur, M.; Yousefi, S.; Meyer, J.P. A new model for density of NFs including nanolayer. *Int. Commun. Heat Mass Transf.* **2016**, *78*, 168–174. [[CrossRef](#)]
- Ghodsinezhad, H.; Sharifpur, M.; Meyer, J.P. Experimental investigation on cavity flow natural convection of Al_2O_3 -water NFs. *Int. Commun. Heat Mass Transf.* **2016**, *76*, 316–324. [[CrossRef](#)]
- Sharifpur, M.; Solomon, A.B.; Ottermann, T.L.; Meyer, J.P. Optimum concentration of NFs for heat transfer enhancement under cavity flow natural convection with TiO_2 -Water. *Int. Commun. Heat Mass Transf.* **2018**, *98*, 297–303. [[CrossRef](#)]

12. Sundar, L.S.; Manoj, A.H.M.; António, K.S.; Hafiz, C.M.S.; Ali, M. Efficiency analysis of thermosyphon solar flat plate collector with low mass concentrations of ND–Co₃O₄ hybrid NFs: An experimental study. *J. Therm. Anal. Calorim.* **2021**, *143*, 959–972. [[CrossRef](#)]
13. Sundar, L.S.; Singh, M.K.; Sousa, A.C.M. Turbulent heat transfer and friction factor of nanodiamond-nickel hybrid NFs flow in a tube: An experimental study. *Int. J. Heat Mass Transf.* **2018**, *117*, 223–234. [[CrossRef](#)]
14. Al-Hossainy, A.F.; Eid, M.R. Combined theoretical and experimental DFT-TDDFT and thermal characteristics of 3-D flow in rotating tube of [PEG + H₂O/SiO₂-Fe₃O₄]C hybrid NF to enhancing oil extraction. *Waves Random Complex Media* **2021**. [[CrossRef](#)]
15. Al-Hossainy, A.F.; Eid, M.R. Combined experimental thin films, TDDFT-DFT theoretical method, and spin effect on [PEG-H₂O/ZrO₂+MgO]h hybrid NF flow with higher chemical rate. *Surf. Interfaces* **2021**, *23*, 100971. [[CrossRef](#)]
16. Eid, M.R.; Al-Hossainy, A.F. High-performance NF synthesis and DFT-TDDFT study of grapheme nanosheets along bent surface for enhanced. *Case Stud. Therm. Eng.* **2021**, *25*, 100983. [[CrossRef](#)]
17. Jamshed, W.; Eid, M.R.; Al-Hossainy, A.F.; Raizah, Z.; Tag El Din, E.S.M.; Sajid, T. Experimental and TDDFT materials simulation of thermal characteristics and entropy optimized of Williamson Cu-methanol and Al₂O₃-methanol NF flowing through solar collector. *Sci. Rep.* **2022**, *12*, 18130. [[CrossRef](#)]
18. Garbadeen, I.D.; Sharifpur, M.; Slabber, J.M.; Meyer, J.P. Experimental study on natural convection of MWCNT-water NFs in a square enclosure. *Int. Commun. Heat Mass Transf.* **2017**, *88*, 1–8. [[CrossRef](#)]
19. Solomon, A.B.; van Rooyen, J.; Rencken, M.; Sharifpur, M.; Meyer, J.P. Experimental study on the influence of the aspect ratio of square cavity on natural convection heat transfer with Al₂O₃/Water NFs. *Int. Commun. Heat Mass Transf.* **2017**, *88*, 254–261. [[CrossRef](#)]
20. Joubert, J.C.; Sharifpur, M.; Solomon, A.B.; Meyer, J.P. Enhancement in heat transfer of a ferrofluid in a differentially heated square cavity through the use of permanent magnets. *J. Magn. Magn. Mater.* **2017**, *443*, 149–158. [[CrossRef](#)]
21. Solomon, A.B.; Sharifpur, M.; Ottermann, T.; Grobler, C.; Joubert, M.; Meyer, J.P. Natural convection enhancement in a porous cavity with Al₂O₃-Ethylene glycol/water NFs. *Int. J. Heat Mass Transf.* **2017**, *108*, 1324–1334. [[CrossRef](#)]
22. Giwa, S.O.; Sharifpur, M.; Meyer, J.P. Heat transfer enhancement of dilute Al₂O₃-MWCNT water based hybrid NFs in a square cavity. In Proceedings of the International Heat Transfer Conference, Beijing, China, 10–15 August 2018; Volume 2018, pp. 5365–5372. [[CrossRef](#)]
23. Waini, I.; Ishak, A.; Grogan, T.; Pop, I. Mixed convection of a hybrid NF flow along a vertical surface embedded in a porous medium. *Int. Commun. Heat Mass Transf.* **2020**, *114*, 104565. [[CrossRef](#)]
24. Alsabery, A.I.; Ismael, M.A.; Chamkha, A.J.; Hashim, I. Mixed convection of Al₂O₃ -water NF in a double lid-driven square cavity with a solid inner insert using Buongiorno's two-phase model. *Int. J. Heat Mass Transf.* **2018**, *119*, 939–961. [[CrossRef](#)]
25. Dalkılıç, A.S.; Türk, O.A.; Mercan, H.; Nakkaew, S.; Wongwises, S. An experimental investigation on heat transfer characteristics of graphite-SiO₂/water hybrid NF flow in horizontal tube with various quad-channel twisted tape inserts. *Int. Commun. Heat Mass Transf.* **2019**, *107*, 1–13. [[CrossRef](#)]
26. Syam Sundar, L.; Otero-Irurueta, G.; Singh, M.K.; Sousa, A.C.M. Heat transfer and friction factor of multi-walled carbon nanotubes-Fe₃O₄ nanocomposite NFs flow in a tube with/without longitudinal strip inserts. *Int. J. Heat Mass Transf.* **2016**, *100*, 691–703. [[CrossRef](#)]
27. Kanti, P.K.; Sharma, K.V.; Minea, A.A.; Kesti, V. Experimental and computational determination of heat transfer, entropy generation and pressure drop under turbulent flow in a tube with fly ash-Cu hybrid NF. *Int. J. Therm. Sci.* **2021**, *167*, 107016. [[CrossRef](#)]
28. Gul, T.; Firdous, K. The experimental study to examine the stable dispersion of the graphene nanoparticles and to look at the GO–H₂O NF flow between two rotating disks. *Appl. Nanosci.* **2018**, *8*, 1711–1727. [[CrossRef](#)]
29. Gul, T.; Khan, M.A.; Noman, W.; Khan, I. SS symmetry Fractional Order Forced Convection Carbon Nanotube NF Flow Passing over a Thin Needle. *Symmetry* **2019**, *11*, 312. [[CrossRef](#)]
30. Sundar, L.S.; Mesfin, S.; Venkata Ramana, E.; Said, Z.; Sousa, A.C.M. Experimental investigation of thermo-physical properties, heat transfer, pumping power, entropy generation, and exergy efficiency of nanodiamond + Fe₃O₄/60, 40% water-ethylene glycol hybrid NF flow in a tube. *Therm. Sci. Eng. Prog.* **2021**, *21*, 100799. [[CrossRef](#)]
31. Mubeen, I.; Shengyong, L.; Jianhua, Y.; Khan, M.S.; Yan, M.; Ali, H.M. Effect of milling material on characteristics and reactivity of mechanically treated fly ash to produce PCDD/F. *J. Therm. Anal. Calorim.* **2021**, *143*, 2707–2716. [[CrossRef](#)]
32. Choudhary, S.; Sachdeva, A.; Kumar, P. Investigation of the stability of MgO NF and its effect on the thermal performance of flat plate solar collector. *Renew. Energy* **2020**, *147*, 1801–1814. [[CrossRef](#)]
33. Okonkwo, E.C.; Wole-Osho, I.; Kavaz, D.; Abid, M.; Al-Ansari, T. Thermodynamic evaluation and optimization of a flat plate collector operating with alumina and iron mono and hybrid NFs. *Sustain. Energy Technol. Assess.* **2020**, *37*, 100636. [[CrossRef](#)]
34. Gopalsamy, V.; Senthil, R.; Varatharajulu, M.; Karunakaran, R. Application of response surface methodology to predict the optimized input quantities of parabolic trough concentrator. *Int. J. Renew. Energy Dev.* **2020**, *9*, 393–400. [[CrossRef](#)]
35. Efemwenkiele, K.U.; Oyedepo, S.O.; Giwa, S.O.; Sharifpur, M.; Owwoeye, T.F.; Akinlabu, K.D.; Meyer, J.P. Experimental investigation of heat transfer performance of novel bio-extract doped mono and hybrid NFs in a radiator. *Case Stud. Therm. Eng.* **2021**, *28*, 101494. [[CrossRef](#)]
36. Khan, A.; Ali, H.M.; Nazir, R.; Ali, R.; Munir, A.; Ahmad, B.; Ahmad, Z. Experimental investigation of enhanced heat transfer of a car radiator using ZnO nanoparticles in H₂O–ethylene glycol mixture. *J. Therm. Anal. Calorim.* **2019**, *138*, 3007–3021. [[CrossRef](#)]

37. Lou, J.F.; Zhang, H.; Wang, R. Experimental investigation of graphite nanolubricant used in a domestic refrigerator. *Adv. Mech. Eng.* **2015**, *7*, 1–9. [[CrossRef](#)]
38. Ho, C.J.; Chen, W.C.; Yan, W.M.; Amani, P. Contribution of hybrid Al₂O₃-water NF and PCM suspension to augment thermal performance of coolant in a minichannel heat sink. *Int. J. Heat Mass Transf.* **2018**, *122*, 651–659. [[CrossRef](#)]
39. Jamil, M.; Khan, A.M.; Hegab, H.; Gong, L.; Mia, M.; Gupta, M.K. Effects of hybrid Al₂O₃-CNT NFs and cryogenic cooling on machining of Ti-6Al-4V. *Int. J. Adv. Manuf. Technol.* **2019**, *102*, 3895–3909. [[CrossRef](#)]
40. Hussien, A.A.; Abdullah, M.Z.; Yusop, N.M.; Al-Nimr, M.A.; Atieh, M.A.; Mehrali, M. Experiment on forced convective heat transfer enhancement using MWCNTs/GNPs hybrid NF and mini-tube. *Int. J. Heat Mass Transf.* **2017**, *115*, 1121–1131. [[CrossRef](#)]
41. Xu, Q.; Liu, L.; Feng, J.; Qiao, L.; Yu, C.; Shi, W.; Ding, C.; Zang, Y.; Chang, C.; Xiong, Y.; et al. A comparative investigation on the effect of different NFs on the thermal performance of two-phase closed thermosyphon. *Int. J. Heat Mass Transf.* **2020**, *149*, 119189. [[CrossRef](#)]
42. Ahmed, F.; Iqbal, M. Heat Transfer Analysis of MHD Power Law Nano Fluid Flow through Annular Sector Duct. *J. Therm. Sci.* **2020**, *29*, 169–181. [[CrossRef](#)]
43. Singh, S.K.; Sarkar, J. Experimental hydrothermal characteristics of concentric tube heat exchanger with V-cut twisted tape turbulator using PCM dispersed mono/hybrid NFs. *Exp. Heat Transf.* **2021**, *34*, 421–442. [[CrossRef](#)]
44. Guo, J.; Barber, G.C.; Schall, D.J.; Zou, Q.; Jacob, S.B. Tribological properties of ZnO and WS₂ NFs using different surfactants. *Wear* **2017**, *382–383*, 8–14. [[CrossRef](#)]
45. Gao, T.; Li, C.; Zhang, Y.; Yang, M.; Jia, D.; Jin, T.; Hou, Y.; Li, R. Dispersing mechanism and tribological performance of vegetable oil-based CNT NFs with different surfactants. *Tribol. Int.* **2019**, *131*, 51–63. [[CrossRef](#)]
46. He, J.; Sun, J.; Meng, Y.; Pei, Y. Superior lubrication performance of MoS₂-Al₂O₃ composite NF in strips hot rolling. *J. Manuf. Process.* **2020**, *57*, 312–323. [[CrossRef](#)]
47. Gugulothu, S.; Pasam, V.K. Experimental investigation to study the performance of CNT/MoS₂ hybrid NF in turning of AISI 1040 steel. *Aust. J. Mech. Eng.* **2020**, *20*, 814–824. [[CrossRef](#)]
48. Ali, M.K.A.; Xianjun, H.; Mai, L.; Qingping, C.; Turkson, R.F.; Bicheng, C. Improving the tribological characteristics of piston ring assembly in automotive engines using Al₂O₃ and TiO₂ nanomaterials as nano-lubricant additives. *Tribol. Int.* **2016**, *103*, 540–554. [[CrossRef](#)]
49. Nam, J.S.; Lee, P.H.; Lee, S.W. Experimental characterization of micro-drilling process using NF minimum quantity lubrication. *Int. J. Mach. Tools Manuf.* **2011**, *51*, 649–652. [[CrossRef](#)]
50. Ali, M.K.A.; Hou, X.; Abdelkareem, M.A.A. Anti-wear properties evaluation of frictional sliding interfaces in automobile engines lubricated by copper/graphene nanolubricants. *Friction* **2020**, *8*, 905–916. [[CrossRef](#)]
51. Ali, M.K.A.; Xianjun, H. Improving the heat transfer capability and thermal stability of vehicle engine oils using Al₂O₃/TiO₂ nanomaterials. *Powder Technol.* **2020**, *363*, 48–58. [[CrossRef](#)]
52. Kiani, M.; Ansari, M.; Arshadi, A.A.; Houshfar, E.; Ashjaee, M. Hybrid thermal management of lithium-ion batteries using NF, metal foam, and phase change material: An integrated numerical-experimental approach. *J. Therm. Anal. Calorim.* **2020**, *141*, 1703–1715. [[CrossRef](#)]
53. Navarrete, N.; Mondragón, R.; Wen, D.; Navarro, M.E.; Ding, Y.; Juliá, J.E. Thermal energy storage of molten salt -based NF containing nano-encapsulated metal alloy phase change materials. *Energy* **2019**, *167*, 912–920. [[CrossRef](#)]
54. Sharma, H.K.; Verma, S.K.; Singh, P.K.; Kumar, S.; Paswan, M.K.; Singhal, P. Performance analysis of paraffin wax as PCM by using hybrid zinc-cobalt-iron oxide nano-fluid on latent heat energy storage system. *Mater. Today Proc.* **2019**, *26*, 1461–1464. [[CrossRef](#)]
55. Zaibudeen, A.W.; Philip, J. Temperature and pH sensor based on functionalized magnetic NF. *Sens. Actuators B Chem.* **2018**, *268*, 338–349. [[CrossRef](#)]
56. Soares, M.C.P.; Rodrigues, M.S.; Schenkel, E.A.; Perli, G.; Silva, W.H.A.; Gomes, M.K.; Fujiwara, E.; Suzuki, C.K. Evaluation of silica NFs in static and dynamic conditions by an optical fiber sensor. *Sensors* **2020**, *20*, 707. [[CrossRef](#)]
57. Abdullah, S.M.; Rafique, S.; Hamdan, K.S.; Roslan, N.A.; Li, L.; Sulaiman, K. Highly sensitive capacitive cell based on a novel CuTsPc-TiO₂ nanocomposite electrolytic solution for low-temperature sensing applications. *Sens. Actuators A Phys.* **2019**, *289*, 94–99. [[CrossRef](#)]
58. Esmailzadeh, F.; Teja, A.S.; Bakhtyari, A. The κ , μ , and cloud points of bentonite NFs with n-pentadecane as the base fluid. *J. Mol. Liq.* **2020**, *300*, 112307. [[CrossRef](#)]
59. Salehnezhad, L.; Heydari, A.; Fattahi, M. Experimental investigation and rheological behaviors of water-based drilling mud contained starch-ZnO NFs through response surface methodology. *J. Mol. Liq.* **2019**, *276*, 417–430. [[CrossRef](#)]
60. Alnarabiji, M.S.; Yahya, N.; Nadeem, S.; Adil, M.; Baig, M.K.; Ben Ghanem, O.; Azizi, K.; Ahmed, S.; Maulianda, B.; Klemeš, J.J.; et al. NF enhanced oil recovery using induced ZnO nanocrystals by electromagnetic energy: M increment. *Fuel* **2018**, *233*, 632–643. [[CrossRef](#)]
61. Li, R.; Jiang, P.; Gao, C.; Huang, F.; Xu, R.; Chen, X. Experimental investigation of silica-based NF enhanced oil recovery: The effect of wettability alteration. *Energy Fuels* **2017**, *31*, 188–197. [[CrossRef](#)]
62. AfzaliTabar, M.; Rashidi, A.; Alaei, M.; Koolivand, H.; Pourhashem, S.; Askari, S. Hybrid of quantum dots for interfacial tension reduction and reservoir alteration wettability for enhanced oil recovery (EOR). *J. Mol. Liq.* **2020**, *307*, 112984. [[CrossRef](#)]

63. Shao, X.-F.; Mo, S.-P.; Chen, Y.; Yin, T.; Yang, Z.; Jia, L.-S.; Cheng, Z.-D. Solidification behavior of hybrid TiO₂ NFs containing nanotubes and nanoplatelets for cold thermal energy storage. *Appl. Therm. Eng.* **2017**, *117*, 427–436. [[CrossRef](#)]
64. Joseph, A.; Sreekumar, S.; Kumar, C.S.S.; Thomas, S. Optimisation of thermo-optical properties of SiO₂/Ag–CuO NF for direct absorption solar collectors. *J. Mol. Liq.* **2019**, *296*, 111986. [[CrossRef](#)]
65. Hormozi, F.; ZareNezhad, B.; Allahyar, H.R. An experimental investigation on the effects of surfactants on the thermal performance of hybrid NFs in helical coil heat exchangers. *Int. Commun. Heat Mass Transf.* **2016**, *78*, 271–276. [[CrossRef](#)]
66. Giwa, S.O.; Sharifpur, M.; Meyer, J.P. Experimental investigation into heat transfer performance of water-based magnetic hybrid NFs in a rectangular cavity exposed to magnetic excitation. *Int. Commun. Heat Mass Transf.* **2020**, *116*, 104698. [[CrossRef](#)]
67. Khooshechin, M.; Fathi, S.; Salimi, F.; Ovaysi, S. The influence of surfactant and ultrasonic processing on improvement of stability and heat transfer coefficient of CuO nanoparticles in the pool boiling. *Int. J. Heat Mass Transf.* **2020**, *154*, 119783. [[CrossRef](#)]
68. Gulzar, O.; Qayoum, A.; Gupta, R. Photo-thermal characteristics of hybrid NFs based on Therminol-55 oil for concentrating solar collectors. *Appl. Nanosci.* **2019**, *9*, 1133–1143. [[CrossRef](#)]
69. Cacula, K.; Buitrago-Sierra, R.; Herrera, B.; Pabón, E.; Murshed, S.M. NFs' stability effects on the thermal performance of heat pipes: A critical review. *J. Therm. Anal. Calorim.* **2019**, *136*, 1597–1614. [[CrossRef](#)]
70. Koçak Soylu, S.; Atmaca, İ.; Asiltürk, M.; Doğan, A. Improving heat transfer performance of an automobile radiator using Cu and Ag doped TiO₂ based NFs. *Appl. Therm. Eng.* **2019**, *157*, 113743. [[CrossRef](#)]
71. Ghafurian, M.M.; Akbari, Z.; Niazmand, H.; Mehrkhah, R.; Wongwises, S.; Mahian, O. Effect of sonication time on the evaporation rate of seawater containing a nanocomposite. *Ultrason. Sonochem.* **2020**, *61*, 104817. [[CrossRef](#)]
72. Abbasi, S.M.; Rashidi, A.; Nemati, A.; Arzani, K. The effect of functionalisation method on the stability and the κ of NF hybrids of carbon nanotubes/gamma alumina. *Ceram. Int.* **2013**, *39*, 3885–3891. [[CrossRef](#)]
73. Zawrah, M.F.; Khatlab, R.M.; Girgis, L.G.; El Daidamony, H.; Abdel Aziz, R.E. Stability and σ of water-base Al₂O₃ NFs for different applications. *HBRC J.* **2016**, *12*, 227–234. [[CrossRef](#)]
74. Adio, S.A.; Sharifpur, M.; Meyer, J.P. Influence of ultrasonication energy on the dispersion consistency of Al₂O₃–glycerol NF based on μ data, and model development for the required ultrasonication energy density. *J. Exp. Nanosci.* **2016**, *11*, 630–649. [[CrossRef](#)]
75. Giwa, S.O.; Sharifpur, M.; Goodarzi, M.; Alsulami, H.; Meyer, J.P. Influence of base fluid, temperature, and concentration on the thermophysical properties of hybrid NFs of alumina–ferrofluid: Experimental data, modeling through enhanced ANN, ANFIS, and curve fitting. *J. Therm. Anal. Calorim.* **2021**, *143*, 4149–4167. [[CrossRef](#)]
76. Giwa, S.O.; Sharifpur, M.; Meyer, J.P.; Wongwises, S.; Mahian, O. Experimental measurement of μ and σ of water-based γ -Al₂O₃/MWCNT hybrid NFs with various particle mass ratios. *J. Therm. Anal. Calorim.* **2021**, *143*, 1037–1050. [[CrossRef](#)]
77. Giwa, S.O.; Momin, M.; Nwaokocha, C.N.; Sharifpur, M.; Meyer, J.P. Influence of nanoparticles size, per cent mass ratio, and temperature on the thermal properties of water-based MgO–ZnO NF: An experimental approach. *J. Therm. Anal. Calorim.* **2021**, *143*, 1063–1079. [[CrossRef](#)]
78. Mousavi, S.M.; Esmailzadeh, F.; Wang, X.P. Effects of temperature and particles volume concentration on the thermophysical properties and the rheological behavior of CuO/MgO/TiO₂ aqueous ternary hybrid NF: Experimental investigation. *J. Therm. Anal. Calorim.* **2019**, *137*, 879–901. [[CrossRef](#)]
79. Aparna, Z.; Michael, M.; Pabi, S.K.; Ghosh, S. K of aqueous Al₂O₃/Ag hybrid nano fluid at different temperatures and volume concentrations: An experimental investigation and development of new correlation function. *Powder Technol.* **2019**, *343*, 714–722. [[CrossRef](#)]
80. Vicki, W.V.; Abdullah, M.Z.; Gunnasegaran, P. Thermophysical properties of Al₂O₃–CuO hybrid NF at different nanoparticle mixture ratio: An experimental approach. *J. Mol. Liq.* **2020**, *1862*, 183135. [[CrossRef](#)]
81. Xian, H.W.; Sidik, N.A.C.; Saidur, R. Impact of different surfactants and ultrasonication time on the stability and thermophysical properties of hybrid NFs. *Int. Commun. Heat Mass Transf.* **2020**, *110*, 104389. [[CrossRef](#)]
82. Nabil, M.F.; Azmi, W.H.; Hamid, K.A.; Mamat, R. Experimental investigation of heat transfer and friction factor of TiO₂–SiO₂ NFs in water:ethylene glycol mixture. *Int. J. Heat Mass Transf.* **2018**, *124*, 1361–1369. [[CrossRef](#)]
83. Michael, M.; Zagabathuni, A.; Sikdar, S.; Pabi, S.K.; Ghosh, S. Effect of dispersion behavior on the heat transfer characteristics of alumina NF: An experimental investigation and development of a new correlation function. *Int. Nano Lett.* **2020**, *10*, 207–217. [[CrossRef](#)]
84. Mousavi, S.M.; Esmailzadeh, F.; Wang, X.P. A detailed investigation on the thermo-physical and rheological behavior of MgO/TiO₂ aqueous dual hybrid NF. *J. Mol. Liq.* **2019**, *282*, 323–339. [[CrossRef](#)]
85. Menbari, A.; Alemrajabi, A.A.; Ghayeb, Y. Investigation on the stability, μ and extinction coefficient of CuO–Al₂O₃/Water binary mixture NF. *Exp. Therm. Fluid Sci.* **2016**, *74*, 122–129. [[CrossRef](#)]
86. Kamalgharibi, M.; Hormozi, F.; Zamzamin, S.A.H.; Sarafraz, M.M. Experimental studies on the stability of CuO nanoparticles dispersed in different base fluids: Influence of stirring, sonication and surface active agents. *Heat Mass Transf. Und. Stoffuebertragung.* **2016**, *52*, 55–62. [[CrossRef](#)]
87. Abadeh, A.; Passandideh-Fard, M.; Maghrebi, M.J.; Mohammadi, M. Stability and magnetization of Fe₃O₄/water NF preparation characteristics using Taguchi method. *J. Therm. Anal. Calorim.* **2019**, *135*, 1323–1334. [[CrossRef](#)]

88. Tiwari, A.K.; Pandya, N.S.; Said, Z.; Öztop, H.F.; Abu-Hamdeh, N. 4S consideration (synthesis, sonication, surfactant, stability) for the κ of CeO₂ with MWCNT and water based hybrid NF: An experimental assessment. *Colloids Surf. A Physicochem. Eng. Asp.* **2021**, *610*, 125918. [[CrossRef](#)]
89. Suhaimi, N.S.; Din, M.F.M.; Ishak, M.T.; Rahman, A.R.A.; Wang, J.; Hassan, M.Z. Performance and limitation of mineral oil-based carbon nanotubes NF in transformer application. *Alex. Eng. J.* **2022**, *61*, 9623–9635. [[CrossRef](#)]
90. Sharifpur, M.; Ghodsinezhad, H.; Meyer, J.P.; Rolfes, H. Investigation on Ultrasonication Energy Density Effect on Characterization of Zinc Oxide (ZnO) NanoParticle Size Distribution with Using Zeta-Sizer. In Proceedings of the 11th International Conference on Heat Transfer, Fluid Mechanics and Thermodynamics, Conference Centre in the Skukuza Rest Camp, Kruger National Park, South Africa, 20–23 July 2015; pp. 211–216.
91. Tiwari, A.K.; Pandya, N.S.; Said, Z.; Chhatbar, S.H.; Al-Turki, Y.A.; Patel, A.R. 3S (Sonication, surfactant, stability) impact on the μ of hybrid NF with different base fluids: An experimental study. *J. Mol. Liq.* **2021**, *329*, 115455. [[CrossRef](#)]
92. Sajid, M.U.; Ali, H.M. K of hybrid NFs: A critical review. *Int. J. Heat Mass Transf.* **2018**, *126*, 211–234. [[CrossRef](#)]
93. Gupta, M.; Singh, V.; Kumar, S.; Kumar, S.; Dilbaghi, N.; Said, Z. Up to date review on the synthesis and thermophysical properties of hybrid NFs. *J. Clean. Prod.* **2018**, *190*, 169–192. [[CrossRef](#)]
94. Nabil, M.F.; Azmi, W.H.; Abdul Hamid, K.; Mamat, R.; Hagos, F.Y. An experimental study on the κ and dynamic μ of TiO₂-SiO₂ NFs in water: Ethylene glycol mixture. *Int. Commun. Heat Mass Transf.* **2017**, *86*, 181–189. [[CrossRef](#)]
95. Ranga Babu, J.A.; Kumar, K.K.; Srinivasa Rao, S. State-of-art review on hybrid NFs. *Renew. Sustain. Energy Rev.* **2017**, *77*, 551–565. [[CrossRef](#)]
96. Kumar, D.D.; Arasu, A.V. A comprehensive review of preparation, characterization, properties and stability of hybrid NFs. *Renew. Sustain. Energy Rev.* **2018**, *81*, 1669–1689. [[CrossRef](#)]
97. Sundar, L.S.; Venkata Ramana, E.; Graça, M.P.F.; Singh, M.K.; Sousa, A.C.M. Nanodiamond-Fe₃O₄ NFs: Preparation and measurement of μ , electrical and thermal conductivities. *Int. Commun. Heat Mass Transf.* **2016**, *73*, 62–74. [[CrossRef](#)]
98. Adio, S.A.; Mehrabi, M.; Sharifpur, M.; Meyer, J.P. Experimental investigation and model development for effective μ of MgO-ethylene glycol NFs by using dimensional analysis, FCM-ANFIS and GA-PNN techniques. *Int. Commun. Heat Mass Transf.* **2016**, *72*, 71–83. [[CrossRef](#)]
99. Kakavandi, A.; Akbari, M. Experimental investigation of κ of NFs containing of hybrid nanoparticles suspended in binary base fluids and propose a new correlation. *Int. J. Heat Mass Transf.* **2018**, *124*, 742–751. [[CrossRef](#)]
100. Sundar, L.S.; Shushmitha, K.; Singh, M.K.; Sousa, A.C.M. Σ enhancement of nanodiamond-nickel (ND-Ni) nanocomposite based magnetic NFs. *Int. Commun. Heat Mass Transf.* **2014**, *57*, 1–7. [[CrossRef](#)]
101. Askari, S.; Koolivand, H.; Pourkhalil, M.; Lotfi, R.; Rashidi, A. Investigation of Fe₃O₄/Graphene nanohybrid heat transfer properties: Experimental approach. *Int. Commun. Heat Mass Transf.* **2017**, *87*, 30–39. [[CrossRef](#)]
102. Nabati Shoghl, S.; Jamali, J.; Keshavarz Moraveji, M. Σ , μ , and density of different NFs: An experimental study. *Exp. Therm. Fluid Sci.* **2016**, *74*, 339–346. [[CrossRef](#)]
103. Said, Z. Thermophysical and optical properties of SWCNTs NFs. *Int. Commun. Heat Mass Transf.* **2016**, *78*, 207–213. [[CrossRef](#)]
104. Alirezaie, A.; Saedodin, S.; Esfe, M.H.; Rostamian, S.H. Investigation of rheological behavior of MWCNT (COOH-functionalized)/MgO-Engine oil hybrid NFs and modelling the results with artificial neural networks. *J. Mol. Liq.* **2017**, *241*, 173–181. [[CrossRef](#)]
105. Kole, M.; Dey, T.K. Effect of aggregation on the μ of copper oxide-gear oil NFs. *Int. J. Therm. Sci.* **2011**, *50*, 1741–1747. [[CrossRef](#)]
106. Wang, X.-J.; Zhu, D.-S.; Yang, S. Investigation of pH and SDBS on enhancement of κ in NFs. *Chem. Phys. Lett.* **2009**, *470*, 107–111. [[CrossRef](#)]
107. Yang, J.-C.; Li, F.-C.; Zhou, W.-W.; He, Y.-R.; Jiang, B.-C. Experimental investigation on the κ and shear μ of viscoelastic-fluid-based NFs. *Int. J. Heat Mass Transf.* **2012**, *55*, 3160–3166. [[CrossRef](#)]
108. Pastoriza-Gallego, M.J.; Lugo, L.; Legido, J.L.; Pineiro, M.M. Enhancement of κ and volumetric behavior of Fe_xO_y NFs. *J. Appl. Phys.* **2011**, *110*, 1–9. [[CrossRef](#)]
109. Ramadhan, A.I.; Azmi, W.H.; Mamat, R.; Hamid, K.A.; Norsakinah, S. Investigation on stability of tri-hybrid NFs in water-ethylene glycol mixture Investigation on stability of tri -hybrid NFs in water- ethylene glycol mixture. *IOP Conf. Ser. Mater. Sci. Eng.* **2019**, *469*, 012068. [[CrossRef](#)]
110. Midhun Mohan, V.; Sajeeb, A.M. Improving the Efficiency of DASC by Adding CeO₂/CuO Hybrid Nanoparticles in Water. *Int. J. Nanosci.* **2018**, *17*, 1–8. [[CrossRef](#)]
111. Ebrahimi, S.; Saghravani, S.F. Influence of magnetic field on the κ of the water based mixed Fe₃O₄/CuO NF. *J. Magn. Magn. Mater.* **2017**, *441*, 366–373. [[CrossRef](#)]
112. Ghadimi, A.; Saidur, R.; Metselaar, H.S.C. A review of NF stability properties and characterization in stationary conditions. *Int. J. Heat Mass Transf.* **2011**, *54*, 4051–4068. [[CrossRef](#)]
113. Chen, L.F.; Cheng, M.; Yang, D.J.; Yang, L. Enhanced K of NF by Synergistic Effect of Multi-Walled Carbon Nanotubes and Fe₂O₃ Nanoparticles. *Appl. Mech. Mater.* **2014**, *548–549*, 118–123. [[CrossRef](#)]
114. Naddaf, A.; Zeinali Heris, S. Experimental study on κ and σ of diesel oil-based NFs of graphene nanoplatelets and carbon nanotubes. *Int. Commun. Heat Mass Transf.* **2018**, *95*, 116–122. [[CrossRef](#)]
115. Hemmat Esfe, M.; Abbasian Arani, A.A.; Rezaie, M.; Yan, W.M.; Karimipour, A. Experimental determination of κ and dynamic μ of Ag-MgO/water hybrid NF. *Int. Commun. Heat Mass Transf.* **2015**, *66*, 189–195. [[CrossRef](#)]

116. Chen, L.; Yu, W.; Xie, H. Enhanced κ of NFs containing Ag/MWNT composites. *Powder Technol.* **2012**, *231*, 18–20. [[CrossRef](#)]
117. Hajiyan, M.; Ebadi, S.; Mahmud, S.; Biglarbegan, M.; Abdullah, H. Experimental investigation of the effect of an external magnetic field on the κ and μ of Fe₃O₄–glycerol. *J. Therm. Anal. Calorim.* **2018**, *1*, 1–14. [[CrossRef](#)]
118. Esmaeili, E.; Ghazanfar Chaydareh, R.; Rounaghi, S.A. The influence of the alternating magnetic field on the convective heat transfer properties of Fe₃O₄-containing NFs through the Neel and Brownian mechanisms. *Appl. Therm. Eng.* **2017**, *110*, 1212–1219. [[CrossRef](#)]
119. Adio, S.A.; Sharifpur, M.; Meyer, J.P. Investigation Into Effective M , Σ , and pH of γ -Al₂O₃-Glycerol NFs in Einstein Concentration Regime. *Heat Transf. Eng.* **2015**, *36*, 1241–1251. [[CrossRef](#)]
120. Adio, S.A.; Sharifpur, M.; Meyer, J.P. Factors affecting the pH and σ of MgO-ethylene glycol NFs. *Bull. Mater. Sci.* **2015**, *38*, 1345–1357. [[CrossRef](#)]
121. Suresh, S.; Venkataraj, K.P.; Selvakumar, P.; Chandrasekar, M. Synthesis of Al₂O₃-Cu/water hybrid NFs using two step method and its thermo physical properties. *Colloids Surf. A Physicochem. Eng. Asp.* **2011**, *388*, 41–48. [[CrossRef](#)]
122. Kumar, V.; Sarkar, J. Numerical and experimental investigations on heat transfer and pressure drop characteristics of Al₂O₃-TiO₂ hybrid NF in minichannel heat sink with different mixture ratio. *Powder Technol.* **2019**, *345*, 717–727. [[CrossRef](#)]
123. Mahbubul, I.M.; Elcioglu, E.B.; Amalina, M.A.; Saidur, R. Stability, thermophysical properties and performance assessment of alumina–water NF with emphasis on ultrasonication and storage period. *Powder Technol.* **2019**, *345*, 668–675. [[CrossRef](#)]
124. Mahbubul, I.M.; Elcioglu, E.B.; Saidur, R.; Amalina, M.A. Optimization of ultrasonication period for better dispersion and stability of TiO₂–water NF. *Ultrason. Sonochem.* **2017**, *37*, 360–367. [[CrossRef](#)] [[PubMed](#)]
125. Sreekumar, S.; Joseph, A.; Sujith Kumar, C.S.; Thomas, S. Investigation on influence of antimony tin oxide/silver NF on direct absorption parabolic solar collector. *J. Clean. Prod.* **2020**, *249*, 119378. [[CrossRef](#)]
126. Cacia, K.; Ordoñez, F.; Zapata, C.; Herrera, B.; Pabón, E.; Buitrago-Sierra, R. Surfactant concentration and pH effects on the zeta potential values of alumina NFs to inspect stability. *Colloids Surf. A Physicochem. Eng. Asp.* **2019**, *583*, 123960. [[CrossRef](#)]
127. Chakraborty, S.; Mukherjee, J.; Manna, M.; Ghosh, P.; Das, S.; Denys, M.B. Effect of Ag nanoparticle addition and ultrasonic treatment on a stable TiO₂ NF. *Ultrason. Sonochem.* **2012**, *19*, 1044–1050. [[CrossRef](#)] [[PubMed](#)]
128. Kumar, V.; Sarkar, J. Experimental hydrothermal characteristics of minichannel heat sink using various types of hybrid NFs. *Adv. Powder Technol.* **2020**, *31*, 621–631. [[CrossRef](#)]
129. Xian-Ju, W.; Xin-Fang, L. Influence of pH on NFs' M and K . *Chin. Phys. Lett.* **2009**, *26*, 056601. [[CrossRef](#)]
130. Momin, G.G. Experimental Investigation of Mixed Convection With Water-Al₂O₃ & Hybrid NF In Inclined Tube For Laminar Flow. *Int. J. Sci. Technol. Res.* **2013**, *2*, 195–202.
131. Akilu, S.; Baheta, A.T.; Mior, M.A.; Minea, A.A.; Sharma, K.V. Properties of glycerol and ethylene glycol mixture based SiO₂-CuO/C hybrid NF for enhanced solar energy transport. *Sol. Energy Mater. Sol. Cells* **2018**, *179*, 118–128. [[CrossRef](#)]
132. Qing, S.H.; Rashmi, W.; Khalid, M.; Gupta, T.C.S.M.; Nabipoor, M.; Hajibeigy, M.T. K and electrical properties of hybrid SiO₂-graphene naphthenic mineral oil NF as potential transformer oil. *Mater. Res. Express* **2017**, *4*, 015504. [[CrossRef](#)]
133. Okonkwo, E.C.; Wole-Osho, I.; Kavaz, D.; Abid, M. Comparison of experimental and theoretical methods of obtaining the thermal properties of alumina/iron mono and hybrid NFs. *J. Mol. Liq.* **2019**, *292*, 111377. [[CrossRef](#)]
134. Menbari, A.; Alemrajabi, A.A.; Ghayeb, Y. Experimental investigation of stability and extinction coefficient of Al₂O₃-CuO binary nanoparticles dispersed in ethylene glycol-water mixture for low-temperature direct absorption solar collectors. *Energy Convers. Manag.* **2016**, *108*, 501–510. [[CrossRef](#)]
135. Menbari, A.; Alemrajabi, A.A.; Rezaei, A. Experimental investigation of thermal performance for direct absorption solar parabolic trough collector (DASPTC) based on binary NFs. *Exp. Therm. Fluid Sci.* **2017**, *80*, 218–227. [[CrossRef](#)]
136. Baby, T.T.; Ramaprabhu, S. Experimental investigation of the thermal transport properties of a carbon nanohybrid dispersed NF. *Nanoscale* **2011**, *3*, 2208. [[CrossRef](#)] [[PubMed](#)]
137. Zawawi, N.N.M.; Azmi, W.H.; Redhwan, A.A.M.; Sharif, M.Z.; Samykano, M. Experimental investigation on thermo-physical properties of metal oxide composite nanolubricants. *Int. J. Refrig.* **2018**, *89*, 11–21. [[CrossRef](#)]
138. Ganguly, S.; Sikdar, S.; Basu, S. Experimental investigation of the effective σ of aluminum oxide NFs. *Powder Technol.* **2009**, *196*, 326–330. [[CrossRef](#)]
139. Ijam, A.; Saidur, R.; Ganesan, P.; Moradi Golsheikh, A. Stability, thermo-physical properties, and σ of graphene oxide-deionized water/ethylene glycol based NF. *Int. J. Heat Mass Transf.* **2015**, *87*, 92–103. [[CrossRef](#)]
140. Sun, B.; Peng, C.; Zuo, R.; Yang, D.; Li, H. Investigation on the flow and convective heat transfer characteristics of NFs in the plate heat exchanger. *Exp. Therm. Fluid Sci.* **2016**, *76*, 75–86. [[CrossRef](#)]
141. Hadadian, M.; Goharshadi, E.K.; Youssefi, A. Σ , κ , and rheological properties of graphene oxide-based NFs. *J. Nanoparticle Res.* **2014**, *16*, 1–17. [[CrossRef](#)]
142. Yu, W.; Xie, H.; Chen, L.; Li, Y. Enhancement of κ of kerosene-based Fe₃O₄ NFs prepared via phase-transfer method. *Colloids Surf. A Physicochem. Eng. Asp.* **2010**, *355*, 109–113. [[CrossRef](#)]
143. Mahrood, M.R.K.; Etemad, S.G.; Bagheri, R. Free convection heat transfer of non Newtonian NFs under constant heat flux condition. *Int. Commun. Heat Mass Transf.* **2011**, *38*, 1449–1454. [[CrossRef](#)]
144. Arani, A.A.A.; Pourmoghadam, F. Experimental investigation of κ behavior of MWCNTs-Al₂O₃/ethylene glycol hybrid NF: Providing new κ correlation. *Heat Mass Transf. Und. Stoffuebertragung.* **2019**, *55*, 2329–2339. [[CrossRef](#)]

145. Babu, S.R.; Rao, G.S. Experimental investigation of natural convective heat transfer using water-alumina NF with taguchi design of experiments. *Int. J. Mech. Eng. Technol.* **2017**, *8*, 795–804.
146. Shahsavar, A.; Salimpour, M.R.; Saghafian, M.; Shafii, M.B. An experimental study on the effect of ultrasonication on κ of ferrofluid loaded with carbon nanotubes. *Thermochim. Acta* **2015**, *617*, 102–110. [\[CrossRef\]](#)
147. Afzal, A.; Khan, S.A.; Ahamed Saleel, C. Role of ultrasonication duration and surfactant on characteristics of ZnO and CuO NFs. *Mater. Res. Express* **2019**, *6*, 1150d8. [\[CrossRef\]](#)
148. Asadi, A.; Alarifi, I.M.; Ali, V.; Nguyen, H.M. An experimental investigation on the effects of ultrasonication time on stability and κ of MWCNT-water NF: Finding the optimum ultrasonication time. *Ultrason. Sonochem.* **2019**, *58*, 104639. [\[CrossRef\]](#)
149. Asadi, A.; Alarifi, I.M. Effects of ultrasonication time on stability, dynamic μ , and pumping power management of MWCNT-water NF: An experimental study. *Sci. Rep.* **2020**, *10*, 15182. [\[CrossRef\]](#)
150. Mahbubul, I.M.; Shahrul, I.M.; Khaleduzzaman, S.S.; Saidur, R.; Amalina, M.A.; Turgut, A. Experimental investigation on effect of ultrasonication duration on colloidal dispersion and thermophysical properties of alumina-water NF. *Int. J. Heat Mass Transf.* **2015**, *88*, 73–81. [\[CrossRef\]](#)
151. Asadi, A.; Asadi, M.; Siahmargoi, M.; Asadi, T.; Gholami Andarati, M. The effect of surfactant and sonication time on the stability and κ of water-based NF containing Mg(OH)₂ nanoparticles: An experimental investigation. *Int. J. Heat Mass Transf.* **2017**, *108*, 191–198. [\[CrossRef\]](#)
152. Seong, H.; Kim, G.; Jeon, J.; Jeong, H.; Noh, J.; Kim, Y.; Kim, H.; Huh, S. Experimental study on characteristics of grinded graphene NFs with surfactants. *Materials* **2018**, *11*, 950. [\[CrossRef\]](#)
153. Wei, H.; Afrand, M.; Kalbasi, R.; Ali, H.M.; Heidarshenas, B.; Rostami, S. The effect of tungsten trioxide nanoparticles on the κ of ethylene glycol under different sonication durations: An experimental examination. *Powder Technol.* **2020**, *374*, 462–469. [\[CrossRef\]](#)
154. Asadikia, A.; Mirjalily, S.A.A.; Nasirizadeh, N.; Kargarsharifabad, H. Characterization of thermal and electrical properties of hybrid NFs prepared with multi-walled carbon nanotubes and Fe₂O₃ nanoparticles. *Int. Commun. Heat Mass Transf.* **2020**, *117*, 104603. [\[CrossRef\]](#)
155. Garg, P.; Alvarado, J.L.; Marsh, C.; Carlson, T.A.; Kessler, D.A.; Annamalai, K. An experimental study on the effect of ultrasonication on μ and heat transfer performance of multi-wall carbon nanotube-based aqueous NFs. *Int. J. Heat Mass Transf.* **2009**, *52*, 5090–5101. [\[CrossRef\]](#)
156. Nasiri, A.; Shariaty-Niasar, M.; Rashidi, A.; Amrollahi, A.; Khodafarin, R. Effect of dispersion method on κ and stability of NF. *Exp. Therm. Fluid Sci.* **2011**, *35*, 717–723. [\[CrossRef\]](#)
157. Ghadimi, A.; Metselaar, I.H. The influence of surfactant and ultrasonic processing on improvement of stability, κ and μ of titania NF. *Exp. Therm. Fluid Sci.* **2013**, *51*, 1–9. [\[CrossRef\]](#)
158. Xia, G.; Jiang, H.; Liu, R.; Zhai, Y. Effects of surfactant on the stability and κ of Al₂O₃/de-ionized water NFs. *Int. J. Therm. Sci.* **2014**, *84*, 118–124. [\[CrossRef\]](#)
159. Sadeghi, R.; Etemad, S.G.; Keshavarzi, E.; Haghshenasfard, M. Investigation of alumina NF stability by UV-vis spectrum. *Microfluid. NFics* **2015**, *18*, 1023–1030. [\[CrossRef\]](#)
160. Yang, Y.; Grulke, E.A.; Zhang, Z.G.; Wu, G. Thermal and rheological properties of carbon nanotube-in-oil dispersions. *J. Appl. Phys.* **2006**, *99*, 114307. [\[CrossRef\]](#)
161. Kole, M.; Dey, T.K. Effect of prolonged ultrasonication on the κ of ZnO-ethylene glycol NFs. *Thermochim. Acta* **2012**, *535*, 58–65. [\[CrossRef\]](#)
162. Yu, J.; Grossiord, N.; Koning, C.E.; Loos, J. Controlling the dispersion of multi-wall carbon nanotubes in aqueous surfactant solution. *Carbon* **2007**, *45*, 618–623. [\[CrossRef\]](#)
163. Ruan, B.; Jacobi, A.M. Ultrasonication effects on thermal and rheological properties of carbon nanotube suspensions. *Nanoscale Res. Lett.* **2012**, *7*, 127. [\[CrossRef\]](#)
164. Li, F.; Li, L.; Zhong, G.; Zhai, Y.; Li, Z. Effects of ultrasonic time, size of aggregates and temperature on the stability and μ of Cu-ethylene glycol (EG) NFs. *Int. J. Heat Mass Transf.* **2019**, *129*, 278–286. [\[CrossRef\]](#)
165. Mahbubul, I.M.; Saidur, R.; Amalina, M.A.; Niza, M.E. Influence of ultrasonication duration on rheological properties of NF: An experimental study with alumina-water NF. *Int. Commun. Heat Mass Transf.* **2016**, *76*, 33–40. [\[CrossRef\]](#)
166. Amrollahi, A.; Hamidi, A.A.; Rashidi, A.M. The effects of temperature, volume fraction and vibration time on the thermo-physical properties of a carbon nanotube suspension (carbon NF). *Nanotechnology* **2008**, *19*, 315701. [\[CrossRef\]](#)
167. Mahbubul, I.M.; Chong, T.H.; Khaleduzzaman, S.S.; Shahrul, I.M.; Saidur, R.; Long, B.D.; Amalina, M.A. Effect of ultrasonication duration on colloidal structure and μ of alumina-water NF. *Ind. Eng. Chem. Res.* **2014**, *53*, 6677–6684. [\[CrossRef\]](#)
168. Mahbubul, I.M.; Saidur, R.; Hepbasli, A.; Amalina, M.A. Experimental investigation of the relation between yield stress and ultrasonication period of NF. *Int. J. Heat Mass Transf.* **2016**, *93*, 1169–1174. [\[CrossRef\]](#)
169. Said, Z.; Aslam Sohail, M.; Walvekar, R.; Liu, C. Impact of sonication durations on thermophysical properties, contact angle and surface tension of f-MWCNTs NF for heat transfer. *J. Mol. Liq.* **2022**, *358*, 119164. [\[CrossRef\]](#)
170. Abubakr, M.; Osman, T.A.; Kishawy, H.A.; Elharouni, F.; Hegab, H.; Esawi, A.M.K. Preparation, characterization, and analysis of multi-walled carbon nanotube-based NF: An aggregate based interpretation. *RSC Adv.* **2021**, *11*, 25561–25574. [\[CrossRef\]](#)
171. Prakash, R.; Chilambarasan, L.; Rajkumar, K. Process Parameters Effect Investigations on M of Water-ethylene Glycol-based α -alumina NFs: An Ultrasonic Experimental and Statistical Approach. *Arab. J. Sci. Eng.* **2021**, *46*, 11909–11921. [\[CrossRef\]](#)

172. Dagdevir, T.; Ozceyhan, V. Optimization of process parameters in terms of stabilization and κ on water based TiO₂ NF preparation by using Taguchi method and Grey relation analysis. *Int. Commun. Heat Mass Transf.* **2021**, *120*, 105047. [[CrossRef](#)]
173. Lee, J.-H.; Hwang, K.S.; Jang, S.P.; Lee, B.H.; Kim, J.H.; Choi, S.U.; Choi, C.J. Effective viscosities and thermal conductivities of aqueous NFs containing low volume concentrations of Al₂O₃ nanoparticles. *Int. J. Heat Mass Transf.* **2008**, *51*, 2651–2656. [[CrossRef](#)]
174. Graves, J.E.; Latvytė, E.; Greenwood, A.; Emekwuru, N.G. Ultrasonic preparation, stability and κ of a capped copper-methanol NF. *Ultrason. Sonochem.* **2019**, *55*, 25–31. [[CrossRef](#)]
175. Yu, H.; Hermann, S.; Schulz, S.E.; Gessner, T.; Dong, Z.; Li, W.J. Optimizing sonication parameters for dispersion of single-walled carbon nanotubes. *Chem. Phys.* **2012**, *408*, 11–16. [[CrossRef](#)]
176. Begum Elcioglu, E.; Murshed, S.M.S. Ultrasonically tuned surface tension and nano-film formation of aqueous ZnO NFs. *Ultrason. Sonochem.* **2021**, *72*, 105424. [[CrossRef](#)]
177. Wang, X.; Li, X.; Yang, S. Influence of pH and SDBS on the stability and κ of NFs. *Energy Fuels* **2009**, *23*, 2684–2689. [[CrossRef](#)]
178. Apmann, K.; Fulmer, R.; Soto, A.; Vafaei, S. K and μ : Review and optimization of effects of nanoparticles. *Materials* **2021**, *14*, 1291. [[CrossRef](#)]
179. Nguyen, V.S.; Rouxel, D.; Hadji, R.; Vincent, B.; Fort, Y. Effect of ultrasonication and dispersion stability on the cluster size of alumina nanoscale particles in aqueous solutions. *Ultrason. Sonochem.* **2011**, *18*, 382–388. [[CrossRef](#)]
180. Kim, H.J.; Lee, S.; Lee, J.; Jang, S.P. Effect of particle shape on suspension stability and thermal conductivities of water-based bohemite alumina nanofluids. *Energy* **2015**, *90*, 1290–1297. [[CrossRef](#)]
181. Ghorabae, H.; Emami, M.R.S.; Shafahi, M. Effect of NF and Surfactant on Thermosyphon Heat Pipe Performance. *Heat Transf. Eng.* **2020**, *41*, 1829–1842. [[CrossRef](#)]
182. Rajendiran, G.; Kuppasamy, V.B.; Shanmugasundaram, S. Experimental investigation of the effects of sonication time and volume concentration on the performance of PVT solar collector. *IET Renew. Power Gener.* **2018**, *12*, 1375–1381. [[CrossRef](#)]
183. Babu, S.R.; Kumar, N.V.A.R.; Babu, P.R. Effect of moisture and sonication time on dielectric strength and heat transfer performance of transformer oil based Al₂O₃ NF. *Int. J. Adv. Technol. Eng. Explor.* **2021**, *8*, 1222–1233. [[CrossRef](#)]
184. Siddiqui, F.R.; Tso, C.Y.; Chan, K.C.; Fu, S.C.; Chao, C.Y.H. On trade-off for dispersion stability and thermal transport of Cu-Al₂O₃ hybrid NF for various mixing ratios. *Int. J. Heat Mass Transf.* **2019**, *132*, 1200–1216. [[CrossRef](#)]
185. Hashemzadeh, S.; Hormozi, F. An experimental study on hydraulic and thermal performances of hybrid NFs in mini-channel. *J. Therm. Anal. Calorim.* **2020**, *140*, 891–903. [[CrossRef](#)]

Disclaimer/Publisher’s Note: The statements, opinions and data contained in all publications are solely those of the individual author(s) and contributor(s) and not of MDPI and/or the editor(s). MDPI and/or the editor(s) disclaim responsibility for any injury to people or property resulting from any ideas, methods, instructions or products referred to in the content.